On the 'Matsubara heating' of overtone intensities and Fermi splittings

Raz L. Benson[1] and Stuart C. Althorpe[1, a)]
Yusuf Hamied Department of Chemistry, University of Cambridge, Lensfield Road, Cambridge, CB2 1EW, United Kingdom.

(Dated: 13 August 2021)

Classical molecular dynamics (MD) and imaginary-time path-integral dynamics methods underestimate the infrared absorption intensities of overtone and combination bands by typically an order of magnitude. Plé *et al.* [J. Chem. Phys. xx, xxx (2021)] have shown that this is because such methods fail to describe the coupling of the centroid to the Matsubara dynamics of the fluctuation modes; classical first-order perturbation theory (PT) applied to the Matsubara dynamics is sufficient to recover most of the lost intensity in simple models, and gives identical results to quantum (Rayleigh–Schrödinger) PT. Here, we show numerically that the results of this analysis can be used as post-processing correction factors, which can be applied to realistic (classical MD or path-integral dynamics) simulations of infared spectra. We find that the correction factors recover most of the lost intensity in the overtone and combination bands of gas-phase water and ammonia, and much of it for liquid water. We then re-derive and confirm the earlier PT analysis by applying canonical PT to Matsubara dynamics, which has the advantage of avoiding secular terms, and gives a simple picture of the perturbed Matsubara dynamics in terms of action-angle variables. Collectively, these variables 'Matsubara heat' the amplitudes of the overtone and combination vibrations of the centroid to what they would be in a classical system with the oscillators (of frequency Ω_i) held at their quantum effective temperatures (of $\hbar\Omega_i \coth(\beta\hbar\Omega_i/2)/2k_{\rm B}$). Numerical calculations show that a similar neglect of 'Matsubara heating' causes path-integral methods to underestimate Fermi resonance splittings.

I. INTRODUCTION

Imaginary-time path-integral dynamics methods[1–11] can be used to include zero-point energy in simulations of vibrational spectra.[9,12–27] When used within their range of applicability,[9,28–30] these methods give typically slightly blueshifted estimates of the fundamental band origins,[31] and good estimates of the intensities. However, path-integral methods fail badly when applied to overtone and combination bands. Unlike fundamental bands, overtone and combination bands show a large quantum effect in being much more intense (typically by an order of magnitude) than their classical counterparts. Path-integral dynamics methods predict reasonable overtone and combination frequencies (although they are typically more blue-shifted than the fundamental frequencies), but they fail completely to account for the quantum increase in the intensities, giving similar results to classical molecular dynamics (MD).[25] It is tempting to blame this failing on the neglect by path-integral dynamics methods of real-time quantum coherence. However, a recent study by Plé *et al.* has shown that the main culprit is the approximations that imaginary-time path-integral methods (and also classical MD) make to the underlying Matsubara dynamics.[32,33]

Matsubara dynamics is a theory which explains how classical dynamics can be combined consistently with quantum Boltzmann statistics. It is derived by assuming that the quantum Boltzmann distribution remains a smooth function of imaginary time. This condition forces the dynamics to become classical, yet quantum Boltzmann–conserving.[28,34,35] Matsubara dynamics is not practical because the fluctuation modes, which describe the dynamics of the shape of the distribution, need to be sampled over a large phase factor. However, it is useful for analysing practical methods such as centroid molecular dynamics (CMD), [thermostatted] ring-polymer molecular dynamics ([T]RPMD) and the planetary model.[8,21,36,37] It was also recently used to devise the quasi-centroid molecular dynamics (QCMD) method,[38] as well as multi-time generalisations of CMD and [T]RPMD.[39] Each of these methods can be obtained by making a (different) drastic approximation to the Matsubara dynamics of the fluctuations, which effectively decouples the dynamics of the fluctuations from that of the centroid: TRPMD does this by converting the fluctuation modes into thermostatted springs, and CMD and QCMD by mean-field averaging over the fluctuations. Classical MD can also be thought of in this way, as a (severe) approximation to Matsubara dynamics in which the fluctuation-dependence of the centroid force is set to zero.

In ref. 32, Plé *et al.* showed that it is precisely these approximations which cause path-integral methods and classical MD to underestimate the intensities of overtone and combination bands (and, paradoxically, to *over*estimate the intensities of difference bands). They showed that, for a system of cubically coupled harmonic oscillators, and with a linear dipole moment, first-order Rayleigh–Schrödinger (RS) perturbation theory (PT) gives a good approximation to the exact quantum intensity, and that perturbed Matsubara dynamics reproduces this intensity exactly (as also does the linearised semiclassical initial value representation (LSC-IVR) method[40–48]). The coupling with the fluctuation modes was found to increase the amplitudes of the overtone and combination vibrations of the centroid, and thus the absorption intensities, to what they would be in a classical system with the oscillators (of frequency Ω_i) held at their quantum effective temperatures $\hbar\Omega_i \coth(\beta\hbar\Omega_i/2)/2k_{\rm B}$.[32] We will refer to this effect below as 'Matsubara heating'.

In Section II of this article, we test whether the PT results of ref. 32 can be used as post-processing correction factors, to recover the quantum intensities of the overtone and combination

a)Electronic mail: sca10@cam.ac.uk

bands. To save computational time, we mainly compare the results of classical MD with exact quantum results (gas-phase water and ammonia) or experiment (liquid water, using the MB-pol and MB-μ surfaces of Paesani and co-workers[17,49–51]), since the correction factor repairs the inensity loss in classical MD calculations in the same way as in path-integral calculations (by accounting for the neglected centroid-fluctuation coupling). However, to demonstrate the quality of the spectrum that is obtained when the correction factor is combined with state-of-the-art path-integral calcuations, we also apply it to the QCMD spectrum of gas-phase water.[52]

Classical PT is well known to be much less straightforward than quantum PT.[53] Plé *et al.* obtained the perturbed Matsubara results by smoothing the quantum Dyson series; this gave secular terms that needed to be discarded.[32] In Section III, we apply canonical PT directly to Matsubara dynamics. This approach avoids the secular terms and obtains perturbed overtone and combination intensities that agree with those of Plé *et al.* A further advantage of the canonical PT derivation is that it gives a clear picture of the perturbed Matsubara dynamics in terms of action-angle variables, and allows one to formalise the notion of a quantum effective temperature.

A related difficulty experienced by path-integral methods in vibrational spectroscopy is predicting Fermi resonance splittings. Tests on simple models have shown that path-integral methods essentially reproduce the classical splittings,[6,32] which agree with the quantum splittings at high temperatures, but underestimate them at low temperatures, predicting an erroneous $T^{1/2}$ dependence.[54] In Section IV, we show numerically that this failing is also caused by the neglect of 'Matsubara heating', whereby the coupling of the fluctuation modes increases the amplitudes of the perturbed centroid vibrations. Further possible examples of dynamics which could be affected by coupling between the centroid and fluctuation modes are discussed briefly in Section V, which concludes the article.

II. INTENSITY CORRECTION FACTOR FOR OVERTONE AND COMBINATION BANDS

A. Rayleigh–Schrödinger derivation

The results derived by Plé *et al.* can be obtained by applying Rayleigh–Schrödinger perturbation theory (PT)[56] to the Hamiltonian

$$\hat{H} = \hat{H}^{(0)} + \varepsilon \hat{V}^{(1)}, \tag{1}$$

where

$$\hat{H}^{(0)} = \frac{1}{2}\sum_{i=1}^{F} (\hat{p}_i^2 + \Omega_i^2 \hat{q}_i^2), \tag{2}$$

$$\hat{V}^{(1)} \equiv V^{(1)}(\hat{\mathbf{q}}) = \frac{1}{6}\sum_{i=1}^{F}\sum_{j=1}^{F}\sum_{k=1}^{F} \eta_{ijk}\hat{q}_i\hat{q}_j\hat{q}_k, \tag{3}$$

and $\hat{\mathbf{q}} = (\hat{q}_1, \ldots, \hat{q}_F)^{\mathrm{T}}$ are the mass-weighted normal-mode position operators of the molecule, with conjugate momentum operators $\hat{\mathbf{p}}$. The constants η_{ijk} are invariant under permutations of indices. As usual in PT, a real, dimensionless constant ε has been factored out of the perturbing potential, and the calculation rests on the assumption that $|\varepsilon|$ is small. It is also assumed that the unperturbed system is non-degenerate. The vibrational states $|\psi_{\mathbf{n}}\rangle$ and energy levels $E_{\mathbf{n}}$ are then approximated in the usual way as

$$|\psi_{\mathbf{n}}\rangle \simeq |\psi_{\mathbf{n}}^{(0)}\rangle + \varepsilon|\psi_{\mathbf{n}}^{(1)}\rangle, \tag{4}$$

and

$$E_{\mathbf{n}} \simeq E_{\mathbf{n}}^{(0)} + \varepsilon E_{\mathbf{n}}^{(1)} = E_{\mathbf{n}}^{(0)}, \tag{5}$$

where the F quantum numbers $\mathbf{n} = (n_1, \ldots, n_F)^{\mathrm{T}}$ specify the vibrational states, and the second equality in Eq. (5) follows because $E_{\mathbf{n}}^{(1)} = 0$ for a cubic perturbation. Thus to first order in ε, the overtone frequencies are exact multiples of the harmonic frequencies and the combination frequencies are linear combinations.

According to Fermi's Golden Rule, the net energy absorption spectrum is given by

$$\begin{aligned} S_{\mathrm{q}}(\beta;\omega) = \frac{2\pi|\mathcal{E}|^2}{\hbar Z_{\mathrm{q}}(\beta)} \sum_{\mathbf{n}}\sum_{\mathbf{n}'} \left(\mathrm{e}^{-\beta E_{\mathbf{n}}} - \mathrm{e}^{-\beta E_{\mathbf{n}'}}\right) \\ \times \left(E_{\mathbf{n}'} - E_{\mathbf{n}}\right)\left|\langle\psi_{\mathbf{n}}|\hat{\mu}|\psi_{\mathbf{n}'}\rangle\right|^2 \delta\left(E_{\mathbf{n}'} - E_{\mathbf{n}} + \hbar\omega\right), \end{aligned} \tag{6}$$

where $\beta = 1/k_{\mathrm{B}}T$, $\mathcal{E}$ is the electric field strength, $Z_{\mathrm{q}}(\beta) = \sum_{\mathbf{n}} \mathrm{e}^{-\beta E_{\mathbf{n}}}$ is the quantum partition function, and $\hat{\mu}$ is the dipole moment operator,[57] which is taken to be

$$\hat{\mu} = \mu(\hat{\mathbf{q}}) = \mu_0 + \boldsymbol{\xi}\cdot\hat{\mathbf{q}}, \tag{7}$$

where $\boldsymbol{\xi} = (\xi_1, \ldots, \xi_F)^{\mathrm{T}}$ and μ_0 are constants.[58] The integrated infrared absorption intensities are then given by[59]

$$\begin{aligned} \mathcal{I}_{\Delta\mathbf{n}}^{[\mathrm{q}]}(\beta) = \frac{2\pi|\mathcal{E}|^2}{\hbar^2 Z_{\mathrm{q}}(\beta)} \sum_{\mathbf{n}\in\mathrm{orig}(\Delta\mathbf{n})} \left(\mathrm{e}^{-\beta E_{\mathbf{n}}} - \mathrm{e}^{-\beta E_{\mathbf{n}+\Delta\mathbf{n}}}\right) \\ \times \left(E_{\mathbf{n}+\Delta\mathbf{n}} - E_{\mathbf{n}}\right)\left|\langle\psi_{\mathbf{n}}|\hat{\mu}|\psi_{\mathbf{n}+\Delta\mathbf{n}}\rangle\right|^2, \end{aligned} \tag{8}$$

where $\Delta\mathbf{n}$ denotes the change in quantum numbers corresponding to a stimulated transition with energy gap $E_{\mathbf{n}+\Delta\mathbf{n}} - E_{\mathbf{n}} = \hbar\Delta\mathbf{n}\cdot\boldsymbol{\Omega}$, and $\mathrm{orig}(\Delta\mathbf{n})$ is the set of possible initial quantum numbers corresponding to a given $\Delta\mathbf{n}$ (of which typically only the lowest-energy states contribute appreciably to the intensity). We will use $\Delta\mathbf{n}$ as a label for absorption bands interchangeably with the more conventional notation $\Delta n_1\nu_1 + \cdots + \Delta n_F\nu_F$ (so that, e.g., $\mathcal{I}_{\Delta\mathbf{n}}^{[\mathrm{q}]} \equiv \mathcal{I}_{\Delta n_1\nu_1+\cdots+\Delta n_F\nu_F}^{[\mathrm{q}]}$), where $\nu_i \simeq \Omega_i/2\pi$ represents the fundamental (ordinary) frequency of mode i.

Because $\hat{V}^{(1)}$ is cubic and $\hat{\mu}$ is linear, the sole effect of the first-order perturbation is to give non-zero $O(\varepsilon^2)$ intensities to the $|\Delta\mathbf{n}| = 2$ first overtones and binary combination and difference bands. The intensities of the fundamental bands are unchanged, as are the intensities of the $|\Delta\mathbf{n}| > 2$ bands (which remain zero). Evaluating the first-order RS wave function and substituting into Eq. (8) gives the $|\Delta\mathbf{n}| = 2$ intensities as

$$\mathcal{I}_{\nu_i\pm\nu_j}^{[\mathrm{q}]}(\beta) = \varepsilon^2 I_{\nu_i\pm\nu_j}^{[\mathrm{q}]}(\beta) + O(\varepsilon^3), \tag{9}$$

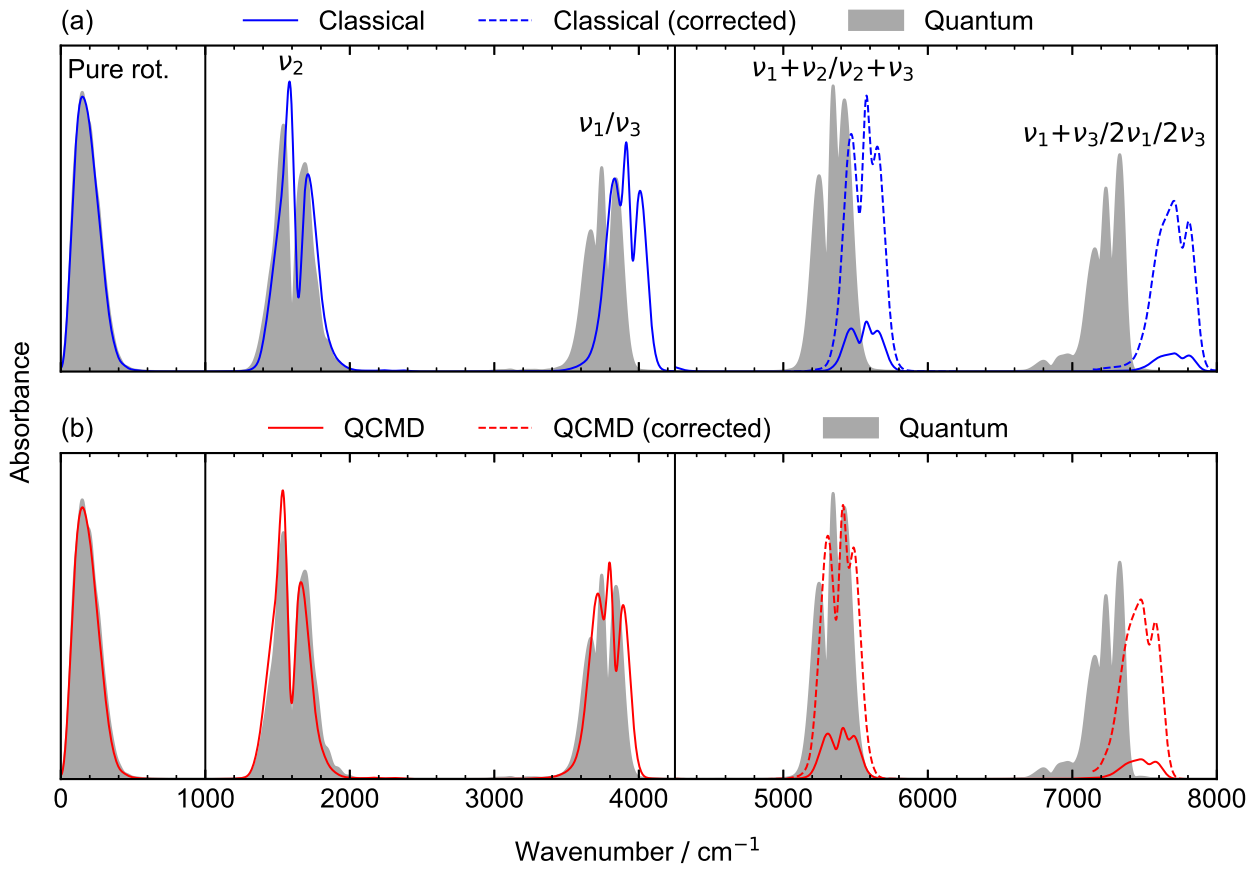

FIG. 1. Damped infrared absorption spectra of gas-phase water at 300 K computed using (a) classical MD and (b) quasi-centroid molecular dynamics (QCMD), compared with quantum results obtained using the code of ref. 55. The dashed lines are obtained by scaling the classical intensities by the 'Matsubara heating' correction factors of Eq. (13), with Ω_i and Ω_j taken to be the mean frequencies of the corresponding fundamental bands. The absorbances in the three panels of the graph are scaled in the ratio 1 : 5 : 70 (left-to-right).

where

$$I^{[\mathrm{q}]}_{\nu_i \pm \nu_j}(\beta) = \frac{1}{2}|\mathcal{E}|^2 \sum_{k=1}^{F}\sum_{l=1}^{F}(2-\delta_{ij})\eta_{ijk}\eta_{ijl}\xi_k\xi_l \times \widetilde{I}^{[\mathrm{q}]}(\beta;\Omega_i,\pm\Omega_j,\Omega_k,\Omega_l) \tag{10}$$

and

$$\widetilde{I}^{[\mathrm{q}]}(\beta;\Omega_i,\Omega_j,\Omega_k,\Omega_l) = \left[\coth\left(\frac{\beta\hbar\Omega_i}{2}\right)+\coth\left(\frac{\beta\hbar\Omega_j}{2}\right)\right] \times \frac{\pi\hbar(\Omega_i+\Omega_j)}{4\Omega_i\Omega_j\left[(\Omega_i+\Omega_j)^2-\Omega_k^2\right]\left[(\Omega_i+\Omega_j)^2-\Omega_l^2\right]}. \tag{11}$$

This is the result derived in ref. 32 (which is equivalent to an expression obtained earlier by Yao and Overend[60]).

We can obtain a quantum–classical correction factor by dividing Eq. (11) by its classical limit,

$$\widetilde{I}^{[\mathrm{c}]}(\beta;\Omega_i,\Omega_j,\Omega_k,\Omega_l) = \lim_{\hbar\to 0}\widetilde{I}^{[\mathrm{q}]}(\beta;\Omega_i,\Omega_j,\Omega_k,\Omega_l) = \frac{\pi(\Omega_i+\Omega_j)^2}{2\beta\Omega_i^2\Omega_j^2\left[(\Omega_i+\Omega_j)^2-\Omega_k^2\right]\left[(\Omega_i+\Omega_j)^2-\Omega_l^2\right]}, \tag{12}$$

to obtain

$$\frac{I^{[\mathrm{q}]}_{\nu_i\pm\nu_j}(\beta)}{I^{[\mathrm{c}]}_{\nu_i\pm\nu_j}(\beta)} = \frac{\beta\hbar\Omega_i\Omega_j}{2(\Omega_i\pm\Omega_j)}\left[\coth\left(\frac{\beta\hbar\Omega_j}{2}\right)\pm\coth\left(\frac{\beta\hbar\Omega_i}{2}\right)\right]. \tag{13}$$

It is easy to show that this correction factor increases the intensities of overtone and combination bands and (somewhat paradoxically) *decreases* the intensities of difference bands.

B. Numerical tests of the intensity correction factor

We carried out numerical tests to determine whether the simple correction factor of Eq. (13) can be used as a post-

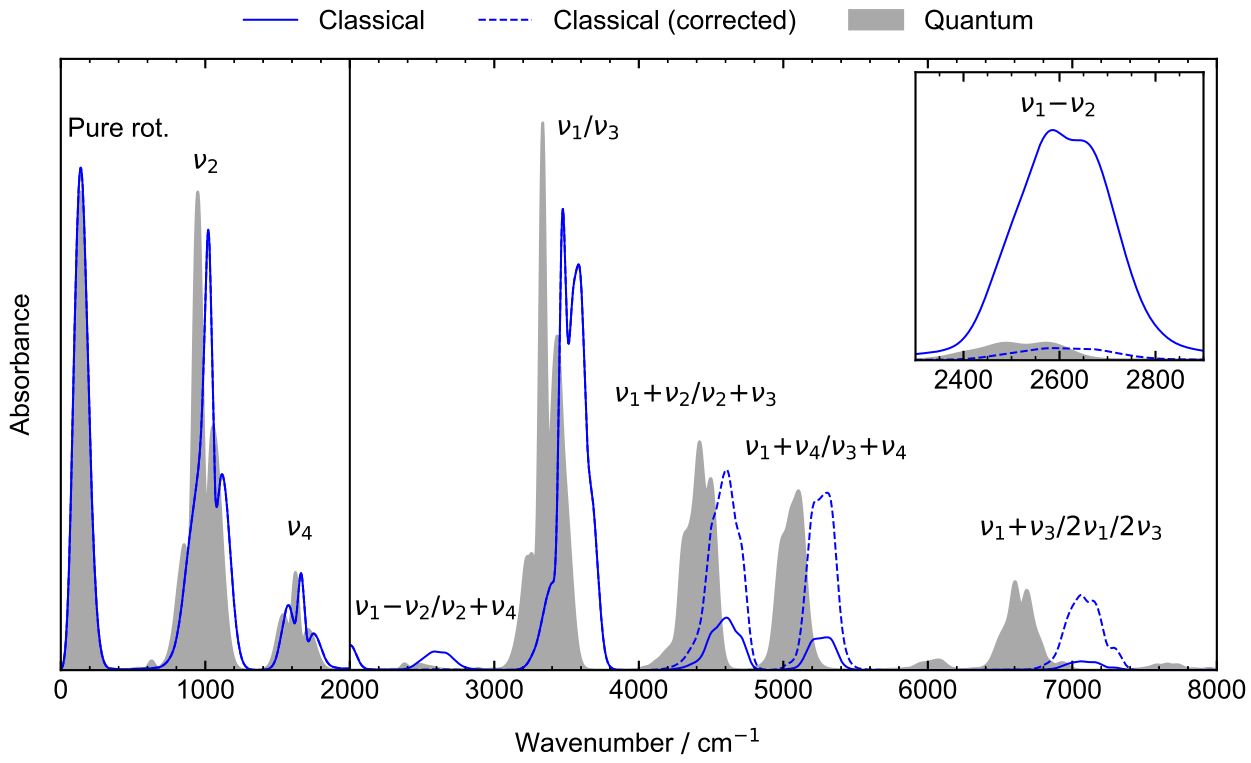

FIG. 2. Damped infrared absorption spectra of gas-phase ammonia at 300 K computed using classical MD, compared with the quantum results of ref. 61. The dashed lines are obtained by scaling the classical intensities by the 'Matsubara heating' correction factors of Eq. (13), as in Fig. 1. Note that the scaling factor *reduces* the intensity of the $\nu_1 - \nu_2$ difference band (see inset). The absorbances in the two panels of the graph are scaled in the ratio 1 : 15 (left-to-right).

processing step to bring the intensities of overtone and combination bands calculated by classical MD or path-integral methods into closer agreement with the quantum intensities.[62]

Fig. 1 compares classical MD, quasi-centroid molecular dynamics (QCMD), and quantum simulations of the infrared spectrum of gas-phase water, computed using the PES[63] and DMS[64] of Partridge and Schwenke. The spectra were damped by convolving with a Hann filter as described in Appendix C (which also gives details of the classical MD simulations and the quantum calculations; the QCMD results are taken from refs. 9 and 25). We assigned the transitions up to $|\Delta\mathbf{n}| = 2$ following ref. 63. As shown in refs. 9 and 25, QCMD improves considerably on classical MD for the positions of the bands, but does not improve on the intensities, which are in good agreement with the quantum results for the fundamentals, but an order of magnitude too small for the overtone and combination bands. However, when Eq. (13) is used to correct the intensities of the latter (taking each Ω_i to be the mean frequency of the corresponding fundamental band or band system), it brings the intensities of these bands into near-quantitative agreement with the quantum results.

As a slightly more challenging test, Fig. 2 shows the same comparison for gas-phase ammonia, calculated using the PES and DMS of Yurchenko *et al.*[61] (see Appendix C for details). We assigned the transitions up to $|\Delta\mathbf{n}| = 2$ following ref. 61. Ammonia has a more crowded non-fundamental spectrum with several systems of overlapping bands, one of which (at 2600 cm^{-1}) includes a difference band. With the exception of two bands at 6000 and 7800 cm^{-1} (which are $|\Delta\mathbf{n}| > 2$ bands and thus not captured by the cubic perturbation), the correction factor again brings the MD intensities into much closer agreement with the quantum results. These include the intensity of the $\nu_1 - \nu_2$ difference band, which is *reduced* from being an order of magnitude too big, to being about 80% of the exact quantum intensity (see Fig. 2 inset, in which the assignments of ref. 61 were used to isolate the $\nu_1 - \nu_2$ contribution to the quantum spectrum).

We would expect Eq. (13) to be much less reliable for the condensed phase, where the intensities are affected by anharmonic coupling through hydrogen bonds; such effects are clearly missing from the simple perturbative model of Eqs. (1–3). Also, bands in the condensed phase often involve overlapping transitions, each of which would require a different correction formula. Nevertheless, Fig. 3 shows that the correction formula gives big improvements to the non-fundamental intensities obtained by applying classical MD to liquid water at 298 K (see Appendix C for numerical details). These corrections were made by treating the 5000 cm^{-1} band as purely a stretch-bend combination, and the 6800 cm^{-1} band as a stretch overtone (with the stretch and bend frequencies taken to be the mean frequencies of the fundamental bands). The quality of the MB-pol PES[49–51] and MB-μ DMS[17] suggest that the

main differences between the MD results and the experimental results of Bertie and Lan[65] arise from the approximate treatment of the quantum statistics and dynamics. The fundamental band intensities are mostly in reasonable agreement with experiment, with the ∼40% underestimate of the integrated stretch intensity probably resulting mostly from neglect of quantum statistical sampling of the non-linear dipole moment (and perhaps partly from the neglect of the bend overtone component). As expected, classical MD strongly underestimates the intensities of the stretch overtone and the bend-libration and stretch-bend combination bands. The correction factor of Eq. (13) brings these intensities much closer to experiment.

III. DERIVATION USING CANONICALLY PERTURBED MATSUBARA DYNAMICS

In ref. 32, Plé *et al.* showed that an identical expression to Eq. (11) can be obtained by applying PT to Matsubara dynamics, by smoothing the Dyson series in imaginary time. Here, we rederive this result by applying canonical PT to Matsubara dynamics, which has the advantages of avoiding secular terms, and interpreting the dynamics in terms of the action-angle variables. We summarise Matsubara dynamics in Section III A, then give the key results of applying canonical PT to a purely classical system in Section III B and to Matsubara dynamics in Section III C. Details of the complete canonical PT derivations are given in Appendices A and B.

A. Summary of Matsubara dynamics

We start with the exact quantum Kubo-transformed dipole moment autocorrelation function (ACF)

$$\widetilde{C}_{\mu\mu}(\beta;t) = \frac{1}{\beta Z_{\mathrm{q}}(\beta)} \int_0^\beta \mathrm{d}\lambda \times \mathrm{Tr}\big[\mathrm{e}^{-(\beta-\lambda)\hat{H}}\hat{\mu}\mathrm{e}^{-\lambda\hat{H}}\mathrm{e}^{\mathrm{i}\hat{H}t/\hbar}\hat{\mu}\mathrm{e}^{-\mathrm{i}\hat{H}t/\hbar}\big], \tag{14}$$

where $\mathrm{Tr}[\dots]$ denotes the quantum mechanical trace and $Z_{\mathrm{q}}(\beta) = \mathrm{Tr}[\mathrm{e}^{-\beta\hat{H}}]$ is the quantum partition function. The (exact) energy absorption spectrum may be obtained from $\widetilde{C}_{\mu\mu}$ using

$$S_{\mathrm{q}}(\beta;\omega) = \beta\omega^2|\mathcal{E}|^2 \int_{-\infty}^{\infty} \mathrm{d}t\ \mathrm{e}^{-\mathrm{i}\omega t}\widetilde{C}_{\mu\mu}(\beta;t), \tag{15}$$

which is equivalent to using Eq. (6) with the exact eigenstates and eigenvalues.[57]

The Matsubara dynamics approximation[34] to $\widetilde{C}_{\mu\mu}$ represents the particles by imaginary-time loops in phase space $(\mathbf{q}(\tau),\mathbf{p}(\tau)) \equiv \{q_i(\tau),p_i(\tau)\}_{i=1}^F$, where $0 < \tau \leq \beta\hbar$ and $\mathbf{q}(\tau) = \mathbf{q}(\tau+\beta\hbar)$ (and similarly for $\mathbf{p}(\tau)$). The loops are smooth functions of τ that can be expanded in terms of M Fourier components

$$\mathbf{Q}_k = \begin{cases} \frac{1}{\beta\hbar}\int_0^{\beta\hbar}\mathrm{d}\tau\mathbf{q}(\tau) & k=0 \\ \frac{\sqrt{2}}{\beta\hbar}\int_0^{\beta\hbar}\mathrm{d}\tau\sin(\omega_k\tau)\mathbf{q}(\tau) & k\in\{1,\dots,\overline{M}\} \\ \frac{\sqrt{2}}{\beta\hbar}\int_0^{\beta\hbar}\mathrm{d}\tau\cos(\omega_k\tau)\mathbf{q}(\tau) & k\in\{-1,\dots,-\overline{M}\}, \end{cases} \tag{16}$$

where $\overline{M} = (M-1)/2$, and

$$\omega_k = \frac{2\pi k}{\beta\hbar} \tag{17}$$

are the Matsubara frequencies.[34] We will refer to $\mathbf{Q}_k \equiv \{Q_{i,k}\}_{i=1}^F$ as the 'Matsubara modes'. The modes $\mathbf{Q}_0$ are the 'centroid' variables, which locate the centres-of-mass of the loops; the other 'non-centroid' or 'fluctuation' modes $\mathbf{Q}_{k\neq0}$ specify the shapes of the loops, and become localised at zero in the high-temperature ($\beta \to 0$) limit. Analogous $\mathbf{P}_k$ are defined in terms of $\mathbf{p}(\tau)$. One can alternatively represent $\mathbf{q}(\tau)$ in terms of the 'bead' coordinates

$$\mathbf{q}_l = \sqrt{M}\sum_{k=-\overline{M}}^{\overline{M}} T_{lk}\mathbf{Q}_k, \quad l\in\{1,\dots,M\} \tag{18}$$

where

$$T_{lk} = \begin{cases} \sqrt{1/M} & k=0 \\ \sqrt{2/M}\sin(2\pi lk/M) & k\in\{1,\dots,\overline{M}\} \\ \sqrt{2/M}\cos(2\pi lk/M) & k\in\{-1,\dots,-\overline{M}\}, \end{cases} \tag{19}$$

such that $\mathbf{q}_l = \mathbf{q}(\tau = l\beta\hbar/M)$; if used to describe a ring-polymer distribution, $q_{i,l}$ would correspond to the l-th ring-polymer bead coordinate of oscillator i.

'Matsubara dynamics' refers to the dynamics within this smooth space, which is classical and generated by the Hamiltonian

$$H_M(\mathbf{P},\mathbf{Q}) = \frac{1}{2}\sum_{k=-\overline{M}}^{\overline{M}}|\mathbf{P}_k|^2 + U_M(\mathbf{Q}), \tag{20}$$

with potential

$$U_M(\mathbf{Q}) = \frac{1}{\beta\hbar}\int_0^{\beta\hbar}\mathrm{d}\tau\ V\big[\mathbf{q}(\tau)\big], \tag{21}$$

where $\mathbf{Q} \equiv \{\mathbf{Q}_k\}_{k=-\overline{M}}^{\overline{M}}$ and similarly for $\mathbf{P}$. We should emphasise that the only approximation made to the dynamics is to have confined it to the smooth space $(\mathbf{P},\mathbf{Q})$; the classicality is entirely a consequence of excluding the non-smooth modes. Such 'jagged' modes (which give the unsmoothed imaginary-time paths a fractal appearance[66]) were shown in ref. 34 to be responsible for real-time quantum coherence.

The Matsubara approximation to $\widetilde{C}_{\mu\mu}$ can be shown to be

$$\widetilde{C}_{\mu\mu}^{[M]}(\beta;t) = \frac{\alpha_M^F}{(2\pi\hbar)^F Z_M(\beta)}\int\mathrm{d}^{FM}\mathbf{P}\int\mathrm{d}^{FM}\mathbf{Q} \times \mathrm{e}^{-\beta[H_M(\mathbf{P},\mathbf{Q})-\mathrm{i}\vartheta_M(\mathbf{P},\mathbf{Q})]}\mu_M(\mathbf{Q})\mathrm{e}^{\mathcal{L}_M t}\mu_M(\mathbf{Q}), \tag{22}$$

where

$$\mathcal{L}_M = \{\cdot, H_M\} = \sum_{k=-\overline{M}}^{\overline{M}}\left[\mathbf{P}_k\cdot\frac{\partial}{\partial\mathbf{Q}_k} - \frac{\partial U_M(\mathbf{Q})}{\partial\mathbf{Q}_k}\cdot\frac{\partial}{\partial\mathbf{P}_k}\right], \tag{23}$$

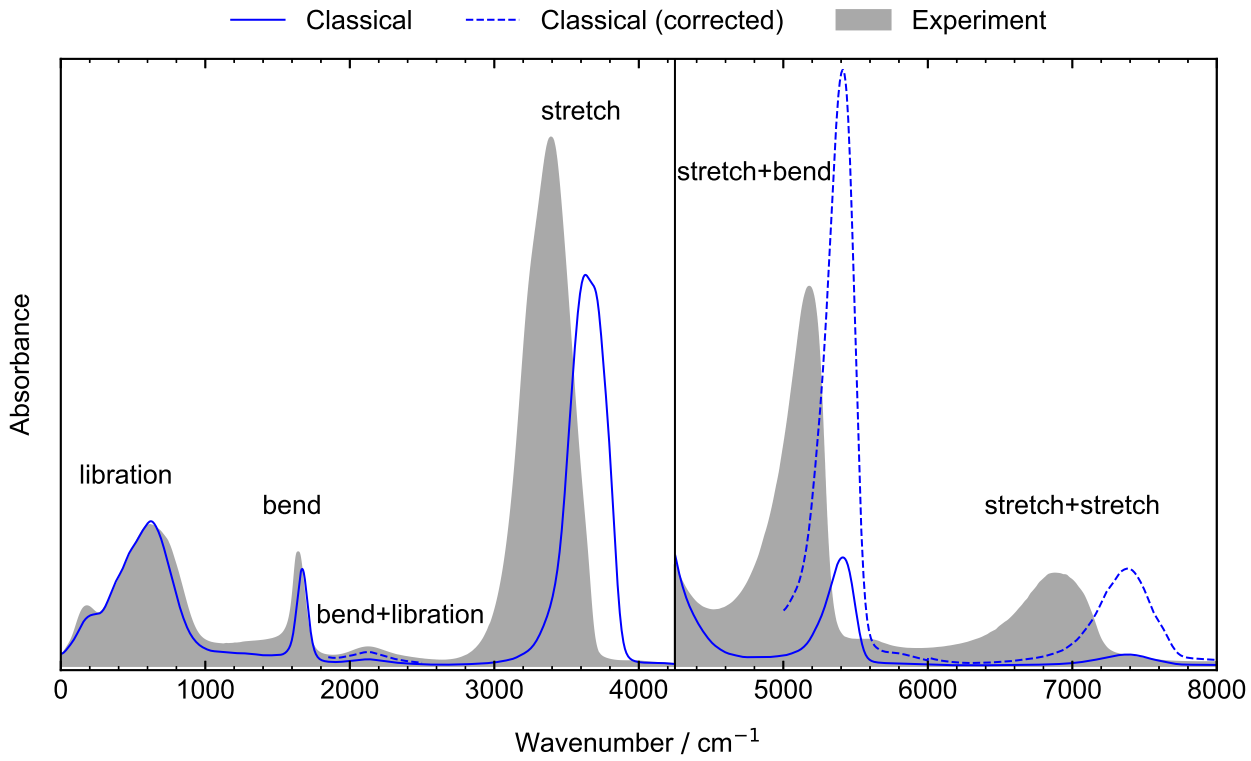

FIG. 3. Infrared absorption spectrum of liquid water at 298 K computed using the MB-pol potential energy surface[49–51] and MB-μ dipole moment surface,[17] compared with the experimental spectrum of ref. 65. The dashed lines are obtained by scaling the classical intensities by the 'Matsubara heating' correction factor of Eq. (13), as in Fig. 1. The absorbances in the two panels of the graph are scaled in the ratio 1 : 70.

$$Z_M(\beta) = \frac{\alpha_M^F}{(2\pi\hbar)^F} \int \mathrm{d}^{FM}\mathbf{P} \int \mathrm{d}^{FM}\mathbf{Q}\, \mathrm{e}^{-\beta[H_M(\mathbf{P},\mathbf{Q})-\mathrm{i}\theta_M(\mathbf{P},\mathbf{Q})]}, \tag{24}$$

and $\alpha_M = \hbar^{1-M}\overline{M}!^2$ is the system-independent contribution to the partition function from the non-smooth modes per physical degree of freedom (which have been integrated out). The dipole moment estimator is

$$\mu_M(\mathbf{Q}) = \frac{1}{\beta\hbar}\int_0^{\beta\hbar} \mathrm{d}\tau\, \mu\big[\mathbf{q}(\tau)\big] \tag{25}$$

in the general case, and reduces to

$$\mu_M(\mathbf{Q}) = \mu_0 + \boldsymbol{\xi}\cdot\mathbf{Q}_0 \tag{26}$$

when the DMS is linear as in the simple model of Eq. (7). The 'Matsubara phase',

$$\theta_M(\mathbf{P},\mathbf{Q}) = \sum_{k=-\overline{M}}^{\overline{M}} \omega_k \mathbf{P}_k\cdot\mathbf{Q}_{-k}, \tag{27}$$

converts the classical-like distribution over $(\mathbf{P},\mathbf{Q})$ into the quantum Boltzmann distribution.[34] The Matsubara phase can be removed by analytic continuation at $t = 0$, where it gives the familiar ring-polymer springs of path-integral MD/MC. But for $t > 0$, the phase cannot be eliminated, which makes the integral in Eq. (22) impossible to sample numerically, except for toy models.

Ring-polymer methods such as CMD, [T]RPMD and QCMD are (drastic) approximations to Matsubara dynamics, which eliminate the phase factor by analytically continuing or averaging over the fluctuation modes. They therefore focus only on the dynamics of the centroid (which does not appear in $\theta_M(\mathbf{P},\mathbf{Q})$).[8,36–38] The simplest approximation to Matsubara dynamics is to set all the fluctuation variables $(\mathbf{P}_k,\mathbf{Q}_k), k\neq 0$ to zero, which recovers the classical time-correlation function

$$C_{\mu\mu}(\beta;t) = \frac{1}{(2\pi\hbar)^F Z_\mathrm{c}(\beta)} \int \mathrm{d}^F\mathbf{p} \int \mathrm{d}^F\mathbf{q}\, \mathrm{e}^{-\beta H(\mathbf{p},\mathbf{q})} \times \mu(\mathbf{q})\mathrm{e}^{\mathcal{L}_\mathrm{c} t}\mu(\mathbf{q}), \tag{28}$$

with

$$Z_\mathrm{c}(\beta) = \frac{1}{(2\pi\hbar)^F} \int \mathrm{d}^F\mathbf{p} \int \mathrm{d}^F\mathbf{q}\, \mathrm{e}^{-\beta H(\mathbf{p},\mathbf{q})}. \tag{29}$$

B. Canonical pertubation theory on the classical system

Let us consider first the $F = 1$ classical counterpart, $H(p,q)$, of $\hat{H}$ in Eq. (1), writing

$$H^{(0)}(p,q) = \frac{1}{2}\big(p^2 + \Omega^2 q^2\big) \tag{30}$$

and

$$V^{(1)}(q) = \frac{1}{6}\eta q^3. \tag{31}$$

The dynamics of the unperturbed oscillator can be described formally using 'action-angle variables' $J^{(0)}$ and $\phi^{(0)}$, which are related to (p, q) by

$$p = \sqrt{2\Omega J^{(0)}}\cos\big(\phi^{(0)}\big) \tag{32a}$$

$$q = \sqrt{\frac{2J^{(0)}}{\Omega}}\sin\big(\phi^{(0)}\big). \tag{32b}$$

The action variable $J^{(0)} = H^{(0)}/\Omega$ is a constant of the motion (of the unperturbed system), whereas the angle $\phi^{(0)}$ evolves according to

$$\phi^{(0)}(t) = \phi^{(0)} + \Omega t \tag{33}$$

and thus describes the phase of the oscillator.[53]

Canonical PT assumes that the perturbed dynamics is describable in terms of a pair of new action-angle variables $(J, \phi) = (J^{(0)}, \phi^{(0)}) + O(\varepsilon)$.[53] By analogy with Eq. (32), we define

$$\varpi = \sqrt{2\Omega J}\cos(\phi) \tag{34a}$$

$$\chi = \sqrt{\frac{2J}{\Omega}}\sin(\phi), \tag{34b}$$

which satisfy $(\varpi, \chi) = (p, q) + O(\varepsilon)$. To lowest order in ε, one can show that

$$\phi(t) = \phi + \Omega t. \tag{35}$$

In other words, when expressed in terms of the new variables (ϖ, χ), the perturbed system oscillates with the same frequency Ω as the unperturbed harmonic oscillator (to lowest order in ε). When expressed in terms of the old variables (p, q), however, the perturbed oscillations have overtone components. In Appendix A, the relation between the old and new variables for the oscillator of Eqs. (30–31) is shown to be

$$q = \sqrt{\frac{2J}{\Omega}}\sin(\phi) - \frac{\varepsilon\eta J}{6\Omega^3}\big[\cos(2\phi) + 3\big] + O(\varepsilon^2). \tag{36}$$

Not surprisingly, q has an $O(\varepsilon^0)$ component oscillating at the fundamental frequency, Ω, and an $O(\varepsilon)$ component at the first overtone frequency, 2Ω.

Writing the $F = 1$ linear dipole of Eq. (7) as

$$\mu = \mu_0 + \xi q, \tag{37}$$

we can substitue q of Eq. (36) into the classical dipole moment ACF of Eq. (28). After Fourier-transforming as in Eq. (15), and integrating over ω, we obtain the classical integrated absorption intensities

$$\mathcal{I}_\nu^{[\mathrm{c}]}(\beta) = \pi\xi^2|\mathcal{E}|^2 + O(\varepsilon) \tag{38}$$

and

$$\mathcal{I}_{2\nu}^{[\mathrm{c}]}(\beta) = \varepsilon^2 I_{2\nu}^{[\mathrm{c}]}(\beta) + O(\varepsilon^3), \tag{39}$$

where (see Appendix A)

$$\begin{aligned} I_{2\nu}^{[\mathrm{c}]}(\beta) &= \frac{\eta^2\xi^2|\mathcal{E}|^2\beta^2}{144\Omega^5}\int \mathrm{d}\varpi \int \mathrm{d}\chi \\ &\quad \times \exp\left\{-\frac{\beta}{2}\left(\varpi^2 + \Omega^2\chi^2\right)\right\}\left(\varpi^2 + \Omega^2\chi^2\right)^2 \end{aligned} \tag{40}$$

$$= \frac{\pi\eta^2\xi^2|\mathcal{E}|^2}{9\beta\Omega^6}. \tag{41}$$

This is identical to the expression for $I_{2\nu}^{[\mathrm{c}]}(\beta)$ given in Eq. (12) (with $F = 1, \Omega_1 = \Omega$).

C. Generalisation to Matsubara dynamics

We now generalise the above treatment to Matsubara dynamics, which we show gives the quantum intensities $I_{2\nu}^{[\mathrm{q}]}(\beta)$ and $I_{\nu_i \pm \nu_j}^{[\mathrm{q}]}(\beta)$ of Eq. (11). The Matsubara Hamiltonian corresponding to the one-dimensional oscillator of Eqs. (30–31) is

$$H_M(\mathbf{P}, \mathbf{Q}) = H_M^{(0)}(\mathbf{P}, \mathbf{Q}) + \varepsilon U_M^{(1)}(\mathbf{Q}), \tag{42}$$

where

$$H_M^{(0)}(\mathbf{P}, \mathbf{Q}) = \frac{1}{2}\sum_{k=-\overline{M}}^{\overline{M}} P_k^2 + \Omega^2 Q_k^2, \tag{43}$$

and the perturbation $U_M^{(1)}(\mathbf{Q})$ is given by subsituting $V[q(\tau)] = \eta q(\tau)^3/6$ into Eq. (25). To describe the dynamics of the unperturbed oscillator, we can introduce M sets of action-angle variables $(\mathcal{J}_k^{(0)}, \varphi_k^{(0)}), k = -\overline{M}, \ldots, \overline{M}$, each of which is related to (P_k, Q_k) by

$$P_k = \sqrt{2\Omega\mathcal{J}_k^{(0)}}\cos\left(\varphi_k^{(0)}\right) \tag{44a}$$

$$Q_k = \sqrt{\frac{2\mathcal{J}_k^{(0)}}{\Omega}}\sin\left(\varphi_k^{(0)}\right). \tag{44b}$$

Clearly, each $\mathcal{J}_k^{(0)}$ is independently a constant of the motion, and the time evolution of each oscillator is given by

$$\varphi_k^{(0)}(t) = \varphi_k^{(0)} + \Omega t. \tag{45}$$

Using canonical PT, we can also describe the perturbed system in terms of M action-angle variables $(\mathcal{J}_k, \varphi_k) = (\mathcal{J}_k^{(0)}, \varphi_k^{(0)}) + O(\varepsilon)$, and by analogy with Eq. (44), we can define

$$\Pi_k = \sqrt{2\Omega\mathcal{J}_k}\cos(\varphi_k), \tag{46a}$$

$$\mathrm{X}_k = \sqrt{\frac{2\mathcal{J}_k}{\Omega}}\sin(\varphi_k), \tag{46b}$$

which satisfy $(\Pi_k, \mathrm{X}_k) = (P_k, Q_k) + O(\varepsilon)$. One can also show that, to lowest order in ε,

$$\varphi_k(t) = \varphi_k + \Omega t. \tag{47}$$

To $O(\varepsilon^0)$, the k-th set of action-angle variables $(\mathcal{J}_k, \varphi_k)$ depend only on the k-th Matsubara mode, but to $O(\varepsilon)$, they depend also on the $k' \neq k$ Matsubara modes. One may therefore refer to $(\mathcal{J}_k, \varphi_k)$ as describing the 'perturbed dynamics of the k-th Matsubara mode', but must bear in mind that the perturbation mixes in contributions from all the other modes. As a result, the centroid coordinate Q_0 can be expected to depend on all of the action-angle variables, not just on $(\mathcal{J}_0, \varphi_0)$. For the one-dimensional oscillator of Eqs. (30–31), this dependence is shown (in Appendix B) to be

$$Q_0 = \sqrt{\frac{2\mathcal{J}_0}{\Omega}}\sin(\varphi_0) - \frac{\varepsilon\eta}{6\Omega^3}\sum_{k=-\overline{M}}^{\overline{M}}\mathcal{J}_k\big[\cos(2\varphi_k)+3\big] + O(\varepsilon^2), \tag{48}$$

which shows that all the modes $k = -\overline{M}, \ldots, \overline{M}$ make equal contributions to the overtone component of Q_0. This symmetric dependence is perhaps to be expected from the form of the perturbative force on the centroid, which is

$$-\frac{\partial U_M(\mathbf{Q})}{\partial Q_0} = -\frac{\eta}{2}\sum_{k=-\overline{M}}^{\overline{M}} Q_k^2. \tag{49}$$

Substituting for Q_0 in Eqs. (22) and (26), taking the Fourier transform using Eq. (15) and integrating over ω, we obtain the integrated absorption intensities

$$\mathcal{I}_\nu^{[M]}(\beta) = \pi\xi^2|\mathcal{E}|^2 + O(\varepsilon) \tag{50}$$

and (see Appendix B)

$$\mathcal{I}_{2\nu}^{[M]}(\beta) = \varepsilon^2 I_{2\nu}^{[M]}(\beta) + O(\varepsilon^3), \tag{51}$$

where

$$I_{2\nu}^{[M]}(\beta) = \frac{\alpha_M\eta^2\xi^2\beta|\mathcal{E}|^2}{144\hbar\Omega^6 Z_M^{(0)}(\beta)}\sum_{k'=-\overline{M}}^{\overline{M}}\sum_{k=-\overline{M}}^{\overline{M}}\int \mathrm{d}^M\mathbf{\Pi}\int \mathrm{d}^M\mathbf{X} \times \mathrm{e}^{-\beta[H_M^{(0)}(\mathbf{\Pi},\mathbf{X}) - \mathrm{i}\theta_M(\mathbf{\Pi},\mathbf{X})]}\big(\Pi_{k'} - \mathrm{i}\Omega\mathrm{X}_{k'}\big)^2\big(\Pi_k + \mathrm{i}\Omega\mathrm{X}_k\big)^2. \tag{52}$$

Defining (ϖ_l, χ_l) to be the perturbed analogues of (p_l, q_l), i.e.

$$\varpi_l = \sqrt{M}\sum_{k=-\overline{M}}^{\overline{M}} T_{lk}\Pi_k \tag{53a}$$

$$\chi_l = \sqrt{M}\sum_{k=-\overline{M}}^{\overline{M}} T_{lk}\mathrm{X}_k, \tag{53b}$$

we show in Appendix B that the integral over action-angle variables can be manipulated to give

$$I_{2\nu}^{[M]}(\beta) = \frac{\eta^2\xi^2|\mathcal{E}|^2\big(\beta^{[M]}\big)^2}{144\Omega^5}\int \mathrm{d}\varpi_0\int \mathrm{d}\chi_0 \times \exp\left\{-\frac{1}{2}\beta^{[M]}\big(\varpi_0^2 + \Omega^2\chi_0^2\big)\right\}\big(\varpi_0^2 + \Omega^2\chi_0^2\big)^2 \tag{54}$$

$$= \frac{\pi\eta^2\xi^2|\mathcal{E}|^2}{9\beta^{[M]}\Omega^6}. \tag{55}$$

This is the same as the classical result Eqs. (40–41), except that β is replaced by an effective inverse temperature $\beta^{[M]}$, defined by

$$\frac{1}{\beta^{[M]}} = \frac{1}{\beta}\sum_{k=-\overline{M}}^{\overline{M}}\frac{\Omega^2}{\Omega^2+\omega_k^2}. \tag{56}$$

We can therefore write

$$I_{2\nu}^{[M]}(\beta) = I_{2\nu}^{[\mathrm{c}]}\big(\beta^{[M]}\big), \tag{57}$$

which in the infinite-mode limit gives the quantum result

$$\lim_{M\to\infty} I_{2\nu}^{[M]}(\beta) = I_{2\nu}^{[\mathrm{c}]}\big(\beta^{[\infty]}\big) = I_{2\nu}^{[\mathrm{q}]}(\beta), \tag{58}$$

since

$$\lim_{M\to\infty}\frac{1}{\beta^{[M]}} = \frac{1}{\beta^{[\infty]}} = \frac{\hbar\Omega}{2}\coth\left(\frac{\beta\hbar\Omega}{2}\right). \tag{59}$$

To generalise this result to combination and difference bands, we first need to generalise the expression for the classical intensity to the scenario in which each normal mode (p_i, q_i) is prepared at a different inverse temperature β_i. As shown in Appendix A, for the second-order intensity this gives

$$I_{\nu_i\pm\nu_j}^{[\mathrm{c}]}(\boldsymbol{\beta}) = \frac{1}{2}|\mathcal{E}|^2\sum_{k=1}^{F}\sum_{l=1}^{F}(2-\delta_{ij})\eta_{ijk}\eta_{ijl}\xi_k\xi_l \times \widetilde{I}^{[\mathrm{c}]}(\boldsymbol{\beta};\Omega_i,\pm\Omega_j,\Omega_k,\Omega_l), \tag{60}$$

where

$$\widetilde{I}^{[\mathrm{c}]}(\boldsymbol{\beta};\Omega_i,\Omega_j,\Omega_k,\Omega_l) = \frac{\pi(\Omega_i+\Omega_j)(\beta_i\Omega_i+\beta_j\Omega_j)}{2\beta_i\beta_j\Omega_i^2\Omega_j^2\big[(\Omega_i+\Omega_j)^2-\Omega_k^2\big]\big[(\Omega_i+\Omega_j)^2-\Omega_l^2\big]} \tag{61}$$

and where we have defined a set of mode-specific inverse temperatures $\boldsymbol{\beta} = (\beta_1, \ldots, \beta_F)^{\mathrm{T}}$. The Matsubara intensity is then related to this generalised classical intensity by

$$I_{\nu_i\pm\nu_j}^{[M]}(\beta) \simeq I_{\nu_i\pm\nu_j}^{[\mathrm{c}]}\big(\boldsymbol{\beta}^{[M]}\big), \tag{62}$$

where

$$\frac{1}{\beta_i^{[M]}} = \frac{1}{\beta}\sum_{k=-\overline{M}}^{\overline{M}}\frac{\Omega_i^2}{\Omega_i^2+\omega_k^2}. \tag{63}$$

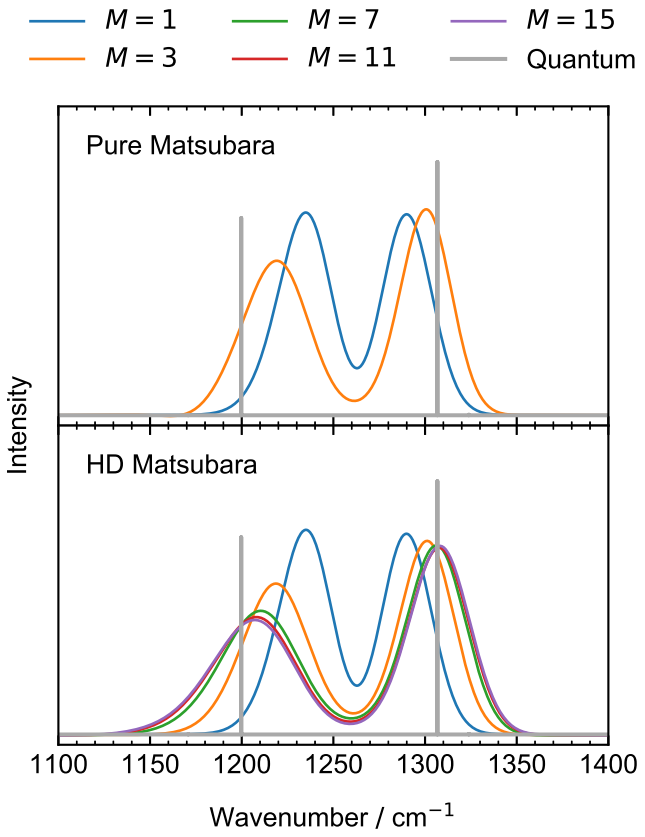

FIG. 4. Velocity autocorrelation spectra of the CO_2 Fermi resonance, computed using the simple model of Eqs. (64–66) at 150 K, using different numbers of Matsubara modes M per physical degree of freedom. The upper panel shows the results of unapproximated Matsubara dynamics calculations, the lower panel the results of using the harmonic decorrelated (HD) approximation to Matsubara dynamics (see Section IV A).

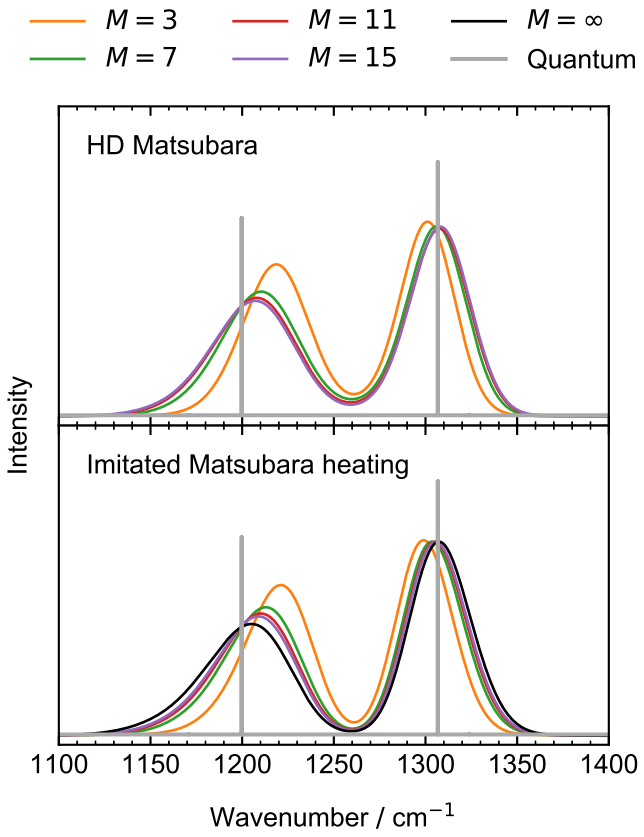

FIG. 5. Same as Fig. 4, with the upper panel showing the results of HD Matsubara dynamics, and the lower panel the results of classical calculations with 'imitated Matsubara heating', in which the oscillators are prepared at the effective inverse temperatures $\beta_i^{[M]}$ (see Section IV B).

The coupling with the fluctuation modes therefore 'Matsubara heats' the amplitudes of the overtone and combination vibrations of the centroid, such that the intensities of the $|\Delta\mathbf{n}| = 2$ bands are the same as what they would be in the classical system if the oscillators were held at the quantum effective temperatures $T_i^{[\infty]} = 1/k_B\beta_i^{[\infty]}$. More formally, the $O(\varepsilon)$ dynamics of the ensemble of perturbed centroid trajectories at temperature T is equivalent to the $O(\varepsilon)$ dynamics of an ensemble of perturbed 'bead' trajectories with the oscillators at their quantum effective temperatures.

IV. FERMI RESONANCES

Fermi resonances occur when a stretch mode of frequency Ω_1 splits by coming into resonance with a bend overtone of frequency $2\Omega_2 \simeq \Omega_1$. A simple model of a Fermi resonance, which is sufficient to demonstrate the failure of classical and path-integral methods to predict the splitting, is[32,54]

$$\hat{H} = \hat{H}^{(0)} + \hat{V}^{(1)}, \tag{64}$$

TABLE I. Parameters used in the CO_2 model Fermi resonance Hamiltonian, taken from ref. 32.

Parameter	Value in atomic units
Ω_1	5.74554×10^{-3}
Ω_2	2.88872×10^{-3}
η_{112}	1.479×10^{-7}

with

$$\hat{H}^{(0)} = \frac{1}{2}\left(\hat{p}_1^2 + \hat{p}_2^2 + \hat{p}_3^2\right) + \frac{1}{2}\Omega_1^2\hat{q}_1^2 + \frac{1}{2}\Omega_2^2\left(\hat{q}_2^2 + \hat{q}_3^2\right) \tag{65}$$

$$\hat{V}^{(1)} = \frac{1}{2}\eta_{122}\hat{q}_1\left(\hat{q}_2^2 + \hat{q}_3^2\right). \tag{66}$$

The numerical values used for Ω_1, Ω_2, and η_{122} are those given in Table I (taken from ref. 32), which model the Fermi resonance in CO_2.

The classical and (Kubo-transformed) quantum velocity autocorrelation spectra[67] of the stretching coordinate q_1 were computed using this model, at a temperature (150 K) for which

the classical Fermi splitting is only 54% of the quantum splitting (see Fig. 4; Matsubara dynamics with $M = 1$ is equivalent to classical dynamics). This underestimation worsens as the temperature is lowered, with the classical splitting scaling as approximately $T^{1/2}$. Only at much higher temperatures (>500 K) do the classical and quantum results agree.[54]

Since Eqs. (64–66) are a special case of Eqs. (1–3) (with $F = 3, \Omega_2 = \Omega_3, \varepsilon = 1$), it seems likely that Matsubara heating (similar to that discussed in Section III) is also responsible for the failure of path-integral methods to reproduce the Fermi splittings. To investigate this, we carried out numerical Matsubara dynamics calculations on the model of Eqs. (64–66).[68]

A. Harmonic decorrelated Matsubara calculations

We first attempted to carry out brute-force Matsubara dynamics simulations of the 150 K Fermi resonance. These calculations were computationally feasible only up to $M = 3$ (a total of 9 Matsubara modes). For $M > 3$, the phase $\theta_M(\mathbf{P}, \mathbf{Q})$ became too oscillatory to integrate over numerically. Nonetheless, including just the $M = 3$ modes is already sufficient to increase the 150 K Fermi splitting from 54% to 76% of the quantum splitting (see Fig. 4).

To include more Matsubara modes in the simulation, we introduce a simple 'harmonic decorrelation' (HD) approximation that allows us to integrate out $\theta_M(\mathbf{P}, \mathbf{Q})$ analytically. The HD approximation is a modification of an approximation introduced in ref. 69. It is based on the observation that, in a harmonic system, the terms

$$\exp\left\{-\frac{\beta}{2}\left(P_{i,k}^2 + \Omega_i^2 Q_{i,-k}^2 - 2\mathrm{i}\omega_k P_{i,k} Q_{i,-k}\right)\right\} \qquad (67)$$

in the quantum Boltzmann distribution can be replaced by the product of the marginal distributions in $P_{i,k}$ and $Q_{i,-k}$,

$$\exp\left\{-\frac{\beta(\Omega_i^2 + \omega_k^2)}{2\Omega_i^2}\left(P_{i,k}^2 + \Omega_i^2 Q_{i,-k}^2\right)\right\}, \qquad (68)$$

provided the function to be integrated over does not contain mixed products of $P_{i,k}$ and $Q_{i,-k}$. We approximate the harmonic parts of the quantum Boltzmann distribution by Eq. (68), but propagate the Matsubara dynamics exactly. We expect this to be a very good approximation for the Fermi resonance model, because the perturbative dependence of the centroid on $P_{i,k}$ and $Q_{i,-k}$ is likely to be dominated by quadratic terms, whereas mixed products involving $P_{i,k}$ and $Q_{i,-k}$ can appear only at quartic or higher powers[70] (which are $O(\eta_{122}^2)$ and thus small).[71]

Fig. 4 shows that the HD approximation yields $M = 3$ Fermi splittings at 150 K that are indistinguishable from those calculated using unapproximated ('pure') Matsubara dynamics. We repeated these calculations with larger values of M, up to $M = 15$ (i.e., a total of 45 Matsubara modes). The addition of each pair of Matsubara modes pushes the HD Matsubara Fermi splitting closer to the exact quantum result, bringing it to within 96% of the quantum splitting by $M = 15$.

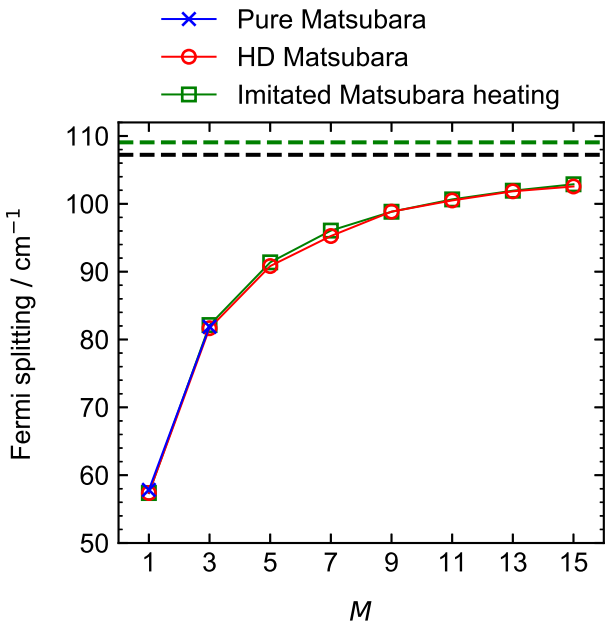

FIG. 6. Fermi splittings as a function of M, defined as the differences between the mean frequencies of the peaks in Figs. 4 and 5 (and including splittings for the intermediate values of M not shown in Figs. 4 and 5). The dashed lines represent the exact quantum splitting (black), and the $M \to \infty$ limit of the imitated Matsubara heating splittings (green).

B. Quantum effective temperatures

In Section III, we showed that the coupling of the Matsubara fluctuation modes to the centroid increases the overtone and combination intensities to what would be obtained from a classical calculation with the oscillators prepared at the quantum effective inverse temperatures $\beta_i^{[\infty]} = 2\tanh(\beta\hbar\Omega_i)/\hbar\Omega_i$. To show that the increase in the Fermi resonance frequency at low temperatures behaves analogously, we plot in Fig. 5 the velocity autocorrelation spectra obtained from purely classical calculations with 'imitated Matsubara heating', in which (p_i, q_i) were sampled from the harmonic oscillator Boltzmann distribution with frequency Ω_i and inverse temperature $\beta_i^{[M]}$ as defined in Eq. (63). For $M = 1$ (not shown), this is equivalent to HD Matsubara dynamics. For $M > 1$, the spectra are still very close to the corresponding HD Matsubara spectra, and the two sets of splittings (plotted against M in Fig. 6) are almost indistinguishable. Fig. 6 also shows that the remaining convergence with respect to $M > 15$ is slow (as expected from the Matsubara convergence 'tails' found in calculations of static properties[66]), but that the $M \to \infty$ limit appears to be tending to within a few cm^{-1} of the exact quantum splitting. To verify this, we repeated the calculations with the oscillators at the quantum effective inverse temperatures $\beta_i^{[\infty]}$, obtaining a Fermi splitting blueshifted by a few cm^{-1} from the exact quantum splitting (see Figs. 5 and 6).

V. CONCLUSIONS

The results of ref. 32 and of this work show that imaginary-time path-integral dynamics methods and classical MD underestimate the vibrational amplitudes of overtone, combination and Fermi resonance vibrations, because they neglect coupling between the Matsubara dynamics of the centroid and the fluctuation modes. In a full Matsubara dynamics calculation, this coupling would increase the amplitudes of the non-fundamental vibrations of the centroid by causing them to resonate in concert with the entire delocalised quantum Boltzmann distribution. This increase in vibrational amplitude magnifies the intensities of overtone and combination bands (typically by an order of magnitude), and increases the widths of Fermi splittings. Real-time coherence (which usually gets the blame when path-integral methods do not work) thus plays no major role here (and treatments more sophisticated than harmonic PT would be required to determine whether it plays a minor role). These findings are consistent with earlier studies based on the LSC-IVR method[72] which, like path-integral methods, omits real-time coherence.[42]

It is probably unrealistic to expect that practical path-integral methods can be generalised to include Matsubara heating, given that the Matsubara fluctuation modes carry large phases. However, the predictions of the cubic perturbation model can be used as post-processing scaling factors, to correct overtone and combination intensities computed using path-integral dynamics methods or classical MD. Clearly one cannot expect quantitative accuracy from a correction based on harmonic perturbation theory, but the results of Section II show that the corrections to the intensities of gas-phase overtone and combination bands are almost quantitative, and that the corrections for liquid water recover much of the lost intensity (including that of the bend-libration combination band, explaining why this band is usually missing from simulated water spectra).[73]

The dynamics responsible for overtones, combination bands and Fermi resonances is by definition anharmonic, and, in the examples discussed above, the dynamics is also (Boltzmann-statistically) highly quantum. We expect that this 'deadly combination' will always cause trouble for path-integral methods, since the Matsubara dynamics will then inevitably couple the centroid with the fluctuation modes, and methods such as TRPMD, CMD and QCMD will therefore not be reliable. This could explain, for example, why TRPMD calculations show large blue shifts in the fundamental bands of highly anharmonic stretch potentials.[23] It may also make it difficult for path-integral methods to compute some (but hopefully not all) of the observables measured by non-linear spectroscopy. This limitation of path-integral methods is only to be expected, given that they were developed to interpolate between dynamics which is either mildly anharmonic and quantum (such as the vibrations of water), or strongly anharmonic and classical (such as the librations in liquid water).

An unanswered question is whether there remain any (significant) observable features in condensed-phase vibrational spectra that one might attribute to real-time coherence. One possible candidate might be the small blueshifts that path-integral methods cannot remove from fundamental stretch peaks,[28] and which tend to be larger (see e.g. Fig. 2 of ref. 25 and Fig. 1 of this article) for overtone and combination bands. Closely related to this are the larger blueshifts found in the protonated water clusters mentioned above. Further work would be needed to determine whether these difficult-to-compute features are caused by real-time coherence, or by coupling of the centroid to the Matsubara fluctuation modes.

ACKNOWLEDGMENTS

We thank Thomas Plé, Simon Huppert, Fabio Finocchi, Philippe Depondt, and Sara Bonella for making available the results of ref. 32 prior to publication, and George Trenins for providing the classical MB-pol/MB-μ liquid water spectrum presented in Fig. 3. R.L.B. gratefully acknowledges the receipt of a studentship from the UK Engineering and Physical Sciences Research Council, award reference 1942965.

SUPPLEMENTARY MATERIAL

See supplementary material for a Mathematica[74] derivation of the Rayleigh–Schrödinger perturbation theory results of Sec. IIA.

DATA AVAILABILITY

The data that support the findings of this study are available from the corresponding author upon reasonable request.

Appendix A: Classical intensities from canonical perturbation theory

In this section, we summarise the standard procedure in multidimensional classical canonical perturbation theory (CPT) and indicate, for completeness, how this may be followed to calculate the second-order classical integrated intensity $I^{[c]}_{\nu_i \pm \nu_j}(\beta)$ directly (rather than taking the classical limit of Eq. (10)). We also show how this procedure can be generalised to the case that each normal mode is prepared at a different temperature.

1. Summary of action-angle variables and classical CPT

Consider the classical analogue of the Hamiltonian in Eq. (1),

$$H(\mathbf{p},\mathbf{q}) = H^{(0)}(\mathbf{p},\mathbf{q}) + \varepsilon V^{(1)}(\mathbf{q}), \tag{A1}$$

with $H^{(0)}$ defined as the classical analogue of Eq. (2) but for now we leave the form of $V^{(1)}$ unspecified. Assuming that the Hamilton–Jacobi equation is completely separable in $(\mathbf{p},\mathbf{q})$,

there exists a set of canonical action-angle variables $(\mathbf{J}, \boldsymbol{\phi})$ with the actions defined by

$$J_i = \frac{1}{2\pi} \oint \mathrm{d}q_i \, p_i, \tag{A2}$$

where $\oint \mathrm{d}q_i$ implies a line integral over a complete period of the orbit in the (p_i, q_i) plane.[53] The Hamiltonian is independent of each conjugate angle ϕ_i and may be written as

$$H(\mathbf{p}, \mathbf{q}) = E(\mathbf{J}). \tag{A3}$$

The classical Liouvillian is thus given by

$$\mathcal{L} = \boldsymbol{\gamma}(\mathbf{J}) \cdot \frac{\partial}{\partial \boldsymbol{\phi}}, \tag{A4}$$

where

$$\boldsymbol{\gamma}(\mathbf{J}) = \frac{\partial E(\mathbf{J})}{\partial \mathbf{J}}, \tag{A5}$$

which implies that each ϕ_i varies linearly in time according to

$$\mathrm{e}^{\mathcal{L}t} \boldsymbol{\phi} = \boldsymbol{\phi} + \boldsymbol{\gamma}(\mathbf{J}) t. \tag{A6}$$

In general, each of the position variables q_i is a periodic function of all $\boldsymbol{\phi}$, with a period of 2π, so q_i may be represented by the Fourier series

$$\mathbf{q} = \sum_{\mathbf{n}} \mathbf{q}_{\mathbf{n}}(\mathbf{J}) \mathrm{e}^{\mathrm{i}\mathbf{n}\cdot\boldsymbol{\phi}}, \tag{A7}$$

and similarly for $\mathbf{p}$. Note that in order for $\mathbf{q}$ to be real, we require $\mathbf{q}_{\mathbf{n}} = \mathbf{q}^*_{-\mathbf{n}}$. The dipole moment, being a function of position, can likewise be expanded as

$$\mu \left[\sum_{\mathbf{n}} \mathbf{q}_{\mathbf{n}}(\mathbf{J}) \mathrm{e}^{\mathrm{i}\mathbf{n}\cdot\boldsymbol{\phi}} \right] = \sum_{\mathbf{n}} \mu_{\mathbf{n}}(\mathbf{J}) \mathrm{e}^{\mathrm{i}\mathbf{n}\cdot\boldsymbol{\phi}}, \tag{A8}$$

where $\mu_{\mathbf{n}} = \mu^*_{-\mathbf{n}}$.

Since the system is non-degenerate we can assume that, as ε approaches zero, the action-angle variables vary smoothly from $(\mathbf{J}, \boldsymbol{\phi})$ to $(\mathbf{J}^{(0)}, \boldsymbol{\phi}^{(0)})$, where

$$p_i = \sqrt{2\Omega_i J_i^{(0)}} \cos\left(\phi_i^{(0)}\right) \tag{A9a}$$

$$q_i = \sqrt{\frac{2J_i^{(0)}}{\Omega_i}} \sin\left(\phi_i^{(0)}\right), \tag{A9b}$$

with

$$H^{(0)}(\mathbf{p}, \mathbf{q}) = E^{(0)}\left(\mathbf{J}^{(0)}\right) = \boldsymbol{\Omega} \cdot \mathbf{J}^{(0)}. \tag{A10}$$

It follows that

$$\boldsymbol{\gamma}(\mathbf{J}) = \boldsymbol{\Omega} + O(\varepsilon). \tag{A11}$$

In classical CPT, one first re-expresses the Hamiltonian in terms of the action-angle variables $(\mathbf{J}^{(0)}, \boldsymbol{\phi}^{(0)})$ for the unperturbed system,[53] giving

$$\widetilde{H}\left(\mathbf{J}^{(0)}, \boldsymbol{\phi}^{(0)}\right) = H(\mathbf{p}, \mathbf{q}) = E^{(0)}\left(\mathbf{J}^{(0)}\right) + \varepsilon \widetilde{V}^{(1)}\left(\mathbf{J}^{(0)}, \boldsymbol{\phi}^{(0)}\right), \tag{A12}$$

where

$$\widetilde{V}^{(1)}\left(\mathbf{J}^{(0)}, \boldsymbol{\phi}^{(0)}\right) = V^{(1)}(\mathbf{p}, \mathbf{q}). \tag{A13}$$

Since p_i and q_i are periodic in $\phi_i^{(0)}$, the perturbation $\widetilde{V}^{(1)}$ must have the Fourier-series representation

$$\widetilde{V}^{(1)}\left(\mathbf{J}^{(0)}, \boldsymbol{\phi}^{(0)}\right) = \sum_{\mathbf{n}} \widetilde{V}^{(1)}_{\mathbf{n}}\left(\mathbf{J}^{(0)}\right) \mathrm{e}^{\mathrm{i}\mathbf{n}\cdot\boldsymbol{\phi}^{(0)}}, \tag{A14}$$

where $\widetilde{V}^{(1)}_{\mathbf{n}} = [\widetilde{V}^{(1)}_{-\mathbf{n}}]^*$. We then assume that the transformed Hamiltonian can be expressed as a power series in ε,

$$E(\mathbf{J}) = \sum_{\alpha=0}^{\infty} \varepsilon^{\alpha} E^{(\alpha)}(\mathbf{J}). \tag{A15}$$

The aim of CPT is to find a series of canonical transformations, starting from $(\mathbf{J}^{(0)}, \boldsymbol{\phi}^{(0)})$, that remove the angle-dependence of the Hamiltonian to progressively higher orders of ε. For our purposes, however, only first-order corrections are required. Introducing the type-II generating function

$$Y\left(\mathbf{J}, \boldsymbol{\phi}^{(0)}\right) = \sum_{\alpha=0}^{\infty} \varepsilon^{\alpha} Y^{(\alpha)}\left(\mathbf{J}, \boldsymbol{\phi}^{(0)}\right), \tag{A16}$$

where

$$Y^{(0)}\left(\mathbf{J}, \boldsymbol{\phi}^{(0)}\right) = \mathbf{J} \cdot \boldsymbol{\phi}^{(0)}, \tag{A17}$$

the perturbed ('new') and unperturbed ('old') variables are related by

$$\mathbf{J}^{(0)} = \frac{\partial Y\left(\mathbf{J}, \boldsymbol{\phi}^{(0)}\right)}{\partial \boldsymbol{\phi}^{(0)}} = \mathbf{J} + \sum_{\alpha=1}^{\infty} \varepsilon^{\alpha} \frac{\partial Y^{(\alpha)}\left(\mathbf{J}, \boldsymbol{\phi}^{(0)}\right)}{\partial \boldsymbol{\phi}^{(0)}} \tag{A18a}$$

$$\boldsymbol{\phi} = \frac{\partial Y\left(\mathbf{J}, \boldsymbol{\phi}^{(0)}\right)}{\partial \mathbf{J}} = \boldsymbol{\phi}^{(0)} + \sum_{\alpha=1}^{\infty} \varepsilon^{\alpha} \frac{\partial Y^{(\alpha)}\left(\mathbf{J}, \boldsymbol{\phi}^{(0)}\right)}{\partial \mathbf{J}}. \tag{A18b}$$

Assuming that each term in the perturbation expansion of $Y\left(\mathbf{J}, \boldsymbol{\phi}^{(0)}\right)$ has a Fourier-series representation

$$Y^{(\alpha)}\left(\mathbf{J}, \boldsymbol{\phi}^{(0)}\right) = \sum_{\mathbf{n}} Y^{(\alpha)}_{\mathbf{n}}(\mathbf{J}) \mathrm{e}^{\mathrm{i}\mathbf{n}\cdot\boldsymbol{\phi}^{(0)}}, \tag{A19}$$

one can show[53] that the coefficients in the first-order term are given by

$$Y^{(1)}_{\mathbf{n}}(\mathbf{J}) = \frac{\mathrm{i}\widetilde{V}^{(1)}_{\mathbf{n}}(\mathbf{J})}{\mathbf{n} \cdot \boldsymbol{\Omega}} \tag{A20}$$

for $\mathbf{n} \neq \mathbf{0}$, and that the first-order energy correction is

$$E^{(1)}(\mathbf{J}) = \widetilde{V}^{(1)}_{\mathbf{0}}(\mathbf{J}), \tag{A21}$$

which is the average of the perturbation over one period of oscillation. The zero-frequency component of the generating function, $Y^{(1)}_{\mathbf{0}}(\mathbf{J})$, gives only a constant phase shift, thus we can choose to set $Y^{(1)}_{\mathbf{0}}(\mathbf{J}) = 0$ without loss of generality. Using

Eq. (A18), the old variables expressed in terms of the new ones are

$$\mathbf{J}^{(0)} = \mathbf{J} - \varepsilon \sum_{\mathbf{n}\neq\mathbf{0}} \mathbf{n}\widetilde{V}^{(1)}_{\mathbf{n}}(\mathbf{J})\frac{\mathrm{e}^{\mathrm{i}\mathbf{n}\cdot\boldsymbol{\phi}}}{\mathbf{n}\cdot\boldsymbol{\Omega}} + O(\varepsilon^2) \tag{A22a}$$

$$\boldsymbol{\phi}^{(0)} = \boldsymbol{\phi} - \mathrm{i}\varepsilon \sum_{\mathbf{n}\neq\mathbf{0}} \frac{\partial \widetilde{V}^{(1)}_{\mathbf{n}}(\mathbf{J})}{\partial \mathbf{J}}\frac{\mathrm{e}^{\mathrm{i}\mathbf{n}\cdot\boldsymbol{\phi}}}{\mathbf{n}\cdot\boldsymbol{\Omega}} + O(\varepsilon^2). \tag{A22b}$$

Finally, these expression can be substituted in Eq. (A9) to obtain the original dynamical variables, $(\mathbf{p},\mathbf{q})$, in terms of the new action-angle variables, $(\mathbf{J},\boldsymbol{\phi})$. For the one-dimensional system of Eqs. (30–31), this procedure generates Eq. (36).

2. Classical integrated absorption intensities

It is convenient to start from the expression for the quantum energy absorption spectrum in terms of the standard quantum ACF, which is

$$S_{\mathrm{q}}(\beta;\omega) = \frac{\omega}{\hbar}|\mathcal{E}|^2(1-\mathrm{e}^{-\beta\hbar\omega})\int_{-\infty}^{\infty}\mathrm{d}t\,\mathrm{e}^{-\mathrm{i}\omega t}C_{\mu\mu}(\beta;t). \tag{A23}$$

Taking the classical limit of Eq. (A23) gives

$$\begin{aligned} S_{\mathrm{c}}(\beta;\omega) &= \lim_{\hbar\to 0} S_{\mathrm{q}}(\beta;\omega) \\ &= \beta\omega^2|\mathcal{E}|^2\int_{-\infty}^{\infty}\mathrm{d}t\,\mathrm{e}^{-\mathrm{i}\omega t}c_{\mu\mu}(\beta;t), \end{aligned} \tag{A24}$$

where

$$\begin{aligned} c_{\mu\mu}(\beta;t) = \frac{1}{(2\pi\hbar)^F Z_{\mathrm{c}}(\beta)}\int \mathrm{d}^F\mathbf{p}\int \mathrm{d}^F\mathbf{q}\,\mathrm{e}^{-\beta H(\mathbf{p},\mathbf{q})} \\ \times \mu(\mathbf{q})\,\mathrm{e}^{\mathcal{L}t}\mu(\mathbf{q}) \end{aligned} \tag{A25}$$

is the classical dipole moment autocorrelation function, with

$$Z_{\mathrm{c}}(\beta) = \frac{1}{(2\pi\hbar)^F}\int \mathrm{d}^F\mathbf{p}\int \mathrm{d}^F\mathbf{q}\,\mathrm{e}^{-\beta H(\mathbf{p},\mathbf{q})}, \tag{A26}$$

and

$$\mathcal{L} = \{\cdot\,, H\} = \mathbf{p}\cdot\frac{\partial}{\partial\mathbf{q}} - \frac{\partial V(\mathbf{q})}{\partial\mathbf{q}}\cdot\frac{\partial}{\partial\mathbf{p}}. \tag{A27}$$

Transforming to action-angle variables $(\mathbf{J},\boldsymbol{\phi})$, and using Liouville's theorem (that the Jacobian for a canonical transformation must be unity), we can also write

$$c_{\mu\mu}(\beta;t) = \frac{1}{\hbar^F Z_{\mathrm{c}}(\beta)}\sum_{\mathbf{n}}\int \mathrm{d}^F\mathbf{J}\,\mathrm{e}^{-\beta E(\mathbf{J})}\left|\mu_{\mathbf{n}}(\mathbf{J})\right|^2\mathrm{e}^{\mathrm{i}\mathbf{n}\cdot\boldsymbol{\gamma}(\mathbf{J})t} \tag{A28}$$

and

$$Z_{\mathrm{c}}(\beta) = \frac{1}{\hbar^F}\int \mathrm{d}^F\mathbf{J}\,\mathrm{e}^{-\beta E(\mathbf{J})}. \tag{A29}$$

Substituting Eq. (A28) into Eq. (A24) gives

$$\begin{aligned} S_{\mathrm{c}}(\beta;\omega) = \frac{2\pi\beta|\mathcal{E}|^2}{\hbar^F Z_{\mathrm{c}}(\beta)}\sum_{\mathbf{n}}\int \mathrm{d}^F\mathbf{J}\,\mathrm{e}^{-\beta E(\mathbf{J})} \\ \times\left|\mu_{\mathbf{n}}(\mathbf{J})\right|^2\left[\mathbf{n}\cdot\boldsymbol{\gamma}(\mathbf{J})\right]^2\delta\left[\omega-\mathbf{n}\cdot\boldsymbol{\gamma}(\mathbf{J})\right], \end{aligned} \tag{A30}$$

from which it follows (relabelling $\mathbf{n}$ as $\Delta\mathbf{n}$) that the integrated classical intensity of an absorption band is given by

$$\begin{aligned} \mathcal{I}^{[\mathrm{c}]}_{\Delta\mathbf{n}}(\beta) &\equiv \mathcal{I}^{[\mathrm{c}]}_{\Delta n_1\nu_1+\cdots+\Delta n_F\nu_F}(\beta) \\ &= \frac{2\pi\beta|\mathcal{E}|^2}{\hbar^F Z_{\mathrm{c}}(\beta)}\int \mathrm{d}^F\mathbf{J}\,\mathrm{e}^{-\beta E(\mathbf{J})}\left|\mu_{\Delta\mathbf{n}}(\mathbf{J})\right|^2\left[\Delta\mathbf{n}\cdot\boldsymbol{\gamma}(\mathbf{J})\right]^2. \end{aligned} \tag{A31}$$

It is evident that the Fourier components of the dipole moment for $|\Delta\mathbf{n}| > 1$ must satisfy $|\mu_{\Delta\mathbf{n}}|^2 = O(\varepsilon^2)$. Thus, for non-fundamental bands, Eq. (A31) simplifies to

$$\mathcal{I}^{[\mathrm{c}]}_{\Delta\mathbf{n}}(\beta) = \varepsilon^2 I^{[\mathrm{c}]}_{\Delta\mathbf{n}}(\beta) + O(\varepsilon^3), \tag{A32}$$

where

$$\begin{aligned} I^{[\mathrm{c}]}_{\Delta\mathbf{n}}(\beta) = \frac{2\pi\beta|\mathcal{E}|^2\left(\Delta\mathbf{n}\cdot\boldsymbol{\Omega}\right)^2}{\hbar^F Z^{(0)}_{\mathrm{c}}(\beta)} \\ \times\int \mathrm{d}^F\mathbf{J}\,\mathrm{e}^{-\beta\boldsymbol{\Omega}\cdot\mathbf{J}}\lim_{\varepsilon\to 0}\frac{1}{\varepsilon^2}\left|\mu_{\Delta\mathbf{n}}(\mathbf{J})\right|^2, \end{aligned} \tag{A33}$$

and

$$Z^{(0)}_{\mathrm{c}}(\beta) = \prod_{i=1}^{F}\frac{1}{\beta\hbar\Omega_i} \tag{A34}$$

is the zeroth-order classical partition function. Because the distribution in Eq. (A33) is factorisable into independent contributions from each oscillator, the expression is easily generalisable to the multi-temperature case, in which each oscillator (J_i,ϕ_i) is prepared with the inverse temperature $\beta_i = 1/k_{\mathrm{B}}T_i$. The zeroth-order partition function becomes

$$Z^{(0)}_{\mathrm{c}}(\boldsymbol{\beta}) = \prod_{i=1}^{F}\frac{1}{\beta_i\hbar\Omega_i}, \tag{A35}$$

and in the integrand of Eq. (A33) we make the replacement

$$\mathrm{e}^{-\beta\boldsymbol{\Omega}\cdot\mathbf{J}} \to \mathrm{e}^{-\mathbf{B}\boldsymbol{\Omega}\cdot\mathbf{J}}, \tag{A36}$$

where $\mathbf{B} = \mathrm{diag}(\boldsymbol{\beta})$. To take care of the frequency-dependent prefactor, we recognise its origin as the classical limit of the $\omega(1-\mathrm{e}^{-\beta\hbar\omega})$ factor that accounts for detailed balance in Eq. (A23). Hence the replacement that we need to make is

$$\begin{aligned} \beta(\Delta\mathbf{n}\cdot\boldsymbol{\Omega})^2 &\to \lim_{\hbar\to 0}\frac{1}{\hbar}\Delta\mathbf{n}\cdot\boldsymbol{\Omega}\left(1-\mathrm{e}^{-\hbar\Delta\mathbf{n}\cdot\mathbf{B}\boldsymbol{\Omega}}\right) \\ &= (\Delta\mathbf{n}\cdot\boldsymbol{\Omega})(\Delta\mathbf{n}\cdot\mathbf{B}\boldsymbol{\Omega}). \end{aligned} \tag{A37}$$

The (second-order) multi-temperature classical intensity is therefore given by

$$\begin{aligned} I^{[\mathrm{c}]}_{\Delta\mathbf{n}}(\boldsymbol{\beta}) = \frac{2\pi|\mathcal{E}|^2\left(\Delta\mathbf{n}\cdot\boldsymbol{\Omega}\right)\left(\Delta\mathbf{n}\cdot\mathbf{B}\boldsymbol{\Omega}\right)}{\hbar^F Z^{(0)}_{\mathrm{c}}(\boldsymbol{\beta})} \\ \times\int \mathrm{d}^F\mathbf{J}\,\mathrm{e}^{-\mathbf{B}\boldsymbol{\Omega}\cdot\mathbf{J}}\lim_{\varepsilon\to 0}\frac{1}{\varepsilon^2}\left|\mu_{\Delta\mathbf{n}}(\mathbf{J})\right|^2 + O(\varepsilon^3). \end{aligned} \tag{A38}$$

3. Application to the $|\Delta\mathbf{n}| = 2$ bands

The cubic perturbation of Eq. (3) may be written in terms of the old action-angle variables as

$$\widetilde{V}(\mathbf{J}^{(0)},\boldsymbol{\phi}^{(0)}) = \frac{\sqrt{2}}{3}\sum_{i=1}^{F}\sum_{j=1}^{F}\sum_{k=1}^{F}\eta_{ijk}\sqrt{\frac{J_i^{(0)}J_j^{(0)}J_k^{(0)}}{\Omega_i\Omega_j\Omega_k}} \times \sin(\phi_i^{(0)})\sin(\phi_j^{(0)})\sin(\phi_k^{(0)}), \tag{A39}$$

giving

$$E^{(1)} = 0 \tag{A40}$$

and

$$J_i^{(0)} = J_i + \frac{\varepsilon}{\sqrt{8}}\sum_{j=1}^{F}\sum_{k=1}^{F}\eta_{ijk}\sqrt{\frac{J_iJ_jJ_k}{\Omega_i\Omega_j\Omega_k}} \times\left[\frac{\sin(\phi_i+\phi_j+\phi_k)}{\Omega_i+\Omega_j+\Omega_k}+\frac{\sin(\phi_i-\phi_j-\phi_k)}{\Omega_i-\Omega_j-\Omega_k}-\frac{\sin(\phi_i+\phi_j-\phi_k)}{\Omega_i+\Omega_j-\Omega_k}-\frac{\sin(\phi_i-\phi_j+\phi_k)}{\Omega_i-\Omega_j+\Omega_k}\right]+O(\varepsilon^2) \tag{A41a}$$

$$\phi_i^{(0)} = \phi_i + \frac{\varepsilon}{\sqrt{32}}\sum_{j=1}^{F}\sum_{k=1}^{F}\eta_{ijk}\sqrt{\frac{J_jJ_k}{\Omega_i\Omega_j\Omega_kJ_i}} \times\left[\frac{\cos(\phi_i+\phi_j+\phi_k)}{\Omega_i+\Omega_j+\Omega_k}+\frac{\cos(\phi_i-\phi_j-\phi_k)}{\Omega_i-\Omega_j-\Omega_k}-\frac{\cos(\phi_i+\phi_j-\phi_k)}{\Omega_i+\Omega_j-\Omega_k}-\frac{\cos(\phi_i-\phi_j+\phi_k)}{\Omega_i-\Omega_j+\Omega_k}\right]+O(\varepsilon^2). \tag{A41b}$$

The position coordinates then become

$$q_k = \sqrt{\frac{2J_k}{\Omega_k}}\sin(\phi_k) - \frac{\varepsilon}{2}\sum_{i=1}^{F}\sum_{j=1}^{F}\eta_{ijk}\sqrt{\frac{J_iJ_j}{\Omega_i\Omega_j}} \times\left[\frac{\cos(\phi_i+\phi_j)}{(\Omega_i+\Omega_j)^2-\Omega_k^2}-\frac{\cos(\phi_i-\phi_j)}{(\Omega_i-\Omega_j)^2-\Omega_k^2}\right] + O(\varepsilon^2). \tag{A42}$$

Using these results with Eq. (A38) gives Eq. (60), which reduces to the classical limit of Eq. (10) in the single-temperature scenario, $\mathbf{B} = \beta\mathbf{I}$.

Appendix B: Matsubara intensities from canonical perturbation theory

1. Matsubara action-angle variables and CPT

Analogous to the multidimensional classical system, let us assume it is possible to define a set of Matsubara action-angle variables $(\mathcal{J},\boldsymbol{\varphi})$, with

$$\mathcal{J}_k = \frac{1}{2\pi}\oint \mathrm{d}Q_kP_k. \tag{B1}$$

$$H_M(\mathbf{P},\mathbf{Q}) = E_M(\mathcal{J}), \tag{B2}$$

$$\mathcal{L}_M = \boldsymbol{\gamma}_M(\mathcal{J})\cdot\frac{\partial}{\partial\boldsymbol{\varphi}}, \tag{B3}$$

$$\theta_M(\mathbf{P},\mathbf{Q}) = \Theta_M(\mathcal{J},\boldsymbol{\varphi}), \tag{B4}$$

$$\mathbf{Q} = \sum_{\mathbf{m}}\mathbf{Q}_{\mathbf{m}}(\mathcal{J})\mathrm{e}^{\mathrm{i}\mathbf{m}\cdot\boldsymbol{\varphi}}, \tag{B5}$$

and

$$\mu_M\left[\sum_{\mathbf{m}}\mathbf{Q}_{\mathbf{m}}(\mathcal{J})\mathrm{e}^{\mathrm{i}\mathbf{m}\cdot\boldsymbol{\varphi}}\right] = \sum_{\mathbf{m}}\mu_{M,\mathbf{m}}(\mathcal{J})\mathrm{e}^{\mathrm{i}\mathbf{m}\cdot\boldsymbol{\varphi}}, \tag{B6}$$

where

$$\boldsymbol{\gamma}_M(\mathcal{J}) = \frac{\partial E_M(\mathcal{J})}{\partial\mathcal{J}}. \tag{B7}$$

The labels $\mathbf{m} = (m_0, m_1, m_{-1}, \ldots, m_{\overline{M}}, m_{-\overline{M}})^{\mathrm{T}}$ take non-negative integer values.

For the unperturbed Matsubara Hamiltonian $H_M^{(0)}(\mathbf{p},\mathbf{q}) = E_M^{(0)}(\mathcal{J}^{(0)})$, we have

$$P_k = \sqrt{2\Omega\mathcal{J}^{(0)}}\cos\left(\varphi_k^{(0)}\right) \tag{B8a}$$

$$Q_k = \sqrt{\frac{2\mathcal{J}_k^{(0)}}{\Omega}}\sin\left(\varphi_k^{(0)}\right), \tag{B8b}$$

with

$$H_M^{(0)}(\mathbf{P},\mathbf{Q}) = E^{(0)}\left(\mathcal{J}^{(0)}\right) = \Omega\sum_{k=-\overline{M}}^{\overline{M}}\mathcal{J}_k. \tag{B9}$$

It follows that

$$\boldsymbol{\gamma}_M(\boldsymbol{\mathcal{J}}) = (\Omega, \ldots, \Omega)^{\mathrm{T}} + O(\varepsilon). \tag{B10}$$

The application of classical CPT to the Matsubara Hamiltonian is, in the general case, complicated by the fact that $\partial E_M^{(0)}(\boldsymbol{\mathcal{J}}^{(0)})/\partial \mathcal{J}_k^{(0)} = \Omega$ is the same for all $k \in \{-\overline{M}, \ldots, \overline{M}\}$, meaning the reference system is degenerate. The arguments outlined in Appendix A can formally break down, with the first-order Fourier coefficients of the generating function

$$Y^{(1)}_{M,\mathbf{m}}(\boldsymbol{\mathcal{J}}) = \frac{\mathrm{i}}{\Omega}\left[\sum_{k=-\overline{M}}^{\overline{M}} m_k\right]^{-1} \widetilde{U}^{(1)}_{M,\mathbf{m}}(\boldsymbol{\mathcal{J}}) \tag{B11}$$

becoming undefined when $\mathbf{m} \in \mathrm{tot}_M(0)$, where Y_M is understood to be the Matsubara analogue of Y from Appendix A and

$$\mathrm{tot}_M(\Delta n) = \left\{\mathbf{m} \;\middle|\; \textstyle\sum_{k=-\overline{M}}^{\overline{M}} m_k = \Delta n\right\}. \tag{B12}$$

However, in the case of cubic perturbations we will find that

$$\forall \mathbf{m} \in \mathrm{tot}_M(0), \widetilde{U}^{(1)}_{M,\mathbf{m}}(\boldsymbol{\mathcal{J}}) = 0, \tag{B13}$$

implying that the resonances are only manifested at second order in ε. We are interested for now only in first-order corrections to the dynamical variables, so it is justified to proceed as if the system were non-resonant. The corresponding zero-frequency components of the generating function will be undetermined in principle, but each of them produces only a constant phase shift and can thus be set to zero without loss of generality i.e.,

$$\forall \mathbf{m} \in \mathrm{tot}_M(0), Y^{(1)}_{M,\mathbf{m}} = 0. \tag{B14}$$

Another important result is that the first-order perturbation to the Matsubara phase vanishes. That is,

$$\Theta_M(\boldsymbol{\mathcal{J}}, \boldsymbol{\varphi}) = \Theta_M^{(0)}(\boldsymbol{\mathcal{J}}, \boldsymbol{\varphi}) + O(\varepsilon^2), \tag{B15}$$

where

$$\begin{aligned}\Theta_M^{(0)}\big(\boldsymbol{\mathcal{J}}^{(0)}, \boldsymbol{\varphi}^{(0)}\big) &= \theta_M(\mathbf{P}, \mathbf{Q}) \\ &= 2\sum_{k=1}^{\overline{M}} \omega_k \sqrt{\mathcal{J}_k^{(0)} \mathcal{J}_{-k}^{(0)}}\, \sin\big(\varphi_{-k}^{(0)} - \varphi_k^{(0)}\big).\end{aligned} \tag{B16}$$

To show this, consider that the phase is itself a constant of the motion. Thus we expect there to exist a canonical transformation from $(\mathbf{P}, \mathbf{Q})$ to a set of action-angle variables $(L, \ldots, \phi_L, \ldots)$, where

$$L = -\frac{\beta\hbar}{2\pi}\Theta_M = \sum_{k=-\overline{M}}^{\overline{M}} k P_{-k} Q_k \tag{B17}$$

is one of the action coordinates and ϕ_L its conjugate angle, such that

$$\frac{\partial}{\partial \phi_L} = \{\cdot\,, L\} = \sum_{k=-\overline{M}}^{\overline{M}} k\left[P_k \frac{\partial}{\partial P_{-k}} + Q_k \frac{\partial}{\partial Q_{-k}}\right]. \tag{B18}$$

The Matsubara coordinates depend on the imaginary-time origin, τ_0, implicitly through

$$\begin{aligned}p(\tau + \tau_0) &= P_0(\tau_0) \\ &\quad + \sqrt{2}\sum_{k=1}^{\overline{M}}\big[P_k(\tau_0)\sin(\omega_k\tau) + P_{-k}(\tau_0)\cos(\omega_k\tau)\big]\end{aligned} \tag{B19a}$$

$$\begin{aligned}q(\tau + \tau_0) &= Q_0(\tau_0) \\ &\quad + \sqrt{2}\sum_{k=1}^{\overline{M}}\big[Q_k(\tau_0)\sin(\omega_k\tau) + Q_{-k}(\tau_0)\cos(\omega_k\tau)\big],\end{aligned} \tag{B19b}$$

from which it follows that

$$P_k(\tau_0) = P_k(0)\cos(\omega_k\tau_0) - P_{-k}(0)\sin(\omega_k\tau_0) \tag{B20a}$$

$$Q_k(\tau_0) = Q_k(0)\cos(\omega_k\tau_0) - Q_{-k}(0)\sin(\omega_k\tau_0), \tag{B20b}$$

and therefore

$$\frac{\partial P_k}{\partial \tau_0} = -\omega_k P_{-k} \tag{B21a}$$

$$\frac{\partial Q_k}{\partial \tau_0} = -\omega_k Q_{-k}. \tag{B21b}$$

By applying the chain rule we can construct an 'imaginary-time Liouvillian',

$$\frac{\partial}{\partial \tau_0} = \sum_{k=-\overline{M}}^{\overline{M}} \omega_k\left[P_k \frac{\partial}{\partial P_{-k}} + Q_k \frac{\partial}{\partial Q_{-k}}\right], \tag{B22}$$

which, when compared with Eq. (B18) implies that

$$\phi_L = \frac{2\pi\tau_0}{\beta\hbar} + \delta_L, \tag{B23}$$

where δ_L is an arbitrary constant phase shift. Since the Matsubara potential is imaginary-time translation invariant, and thus independent of ϕ_L, Eq. (B15) follows from Eq. (A22a).

2. Matsubara integrated absorption intensities

In terms of action-angle coordinates, the Matsubara approximation to the Kubo-transformed ACF is

$$\begin{aligned}\widetilde{C}^{[M]}_{\mu\mu}(\beta; t) = \frac{\alpha_M}{2\pi\hbar Z_M(\beta)} \sum_{\mathbf{m},\mathbf{m}'} \int \mathrm{d}^M\boldsymbol{\mathcal{J}} \int \mathrm{d}^M\boldsymbol{\varphi} \\ \times \mathrm{e}^{-\beta[E_M(\boldsymbol{\mathcal{J}}) - \mathrm{i}\Theta_M(\boldsymbol{\mathcal{J}},\boldsymbol{\varphi})]} \mu^*_{M,\mathbf{m}'}(\boldsymbol{\mathcal{J}})\mu_{M,\mathbf{m}}(\boldsymbol{\mathcal{J}}) \\ \times \mathrm{e}^{\mathrm{i}(\mathbf{m}-\mathbf{m}')\cdot\boldsymbol{\varphi}} \mathrm{e}^{\mathrm{i}\mathbf{m}\cdot\boldsymbol{\gamma}_M(\boldsymbol{\mathcal{J}})t}\end{aligned} \tag{B24}$$

with

$$Z_M(\beta) = \frac{\alpha_M}{2\pi\hbar}\sum_{\mathbf{m},\mathbf{m}'}\int \mathrm{d}^M\mathcal{J}\int \mathrm{d}^M\boldsymbol{\varphi}\; \mathrm{e}^{-\beta[E_M(\mathcal{J})-\mathrm{i}\Theta_M(\mathcal{J},\boldsymbol{\varphi})]}, \tag{B25}$$

from which it follows that the energy absorption spectrum is given by

$$\begin{aligned} S_M(\beta;\omega) = \frac{\alpha_M\beta|\mathcal{E}|^2}{\hbar Z_M(\beta)}\sum_{\mathbf{m},\mathbf{m}'}\int \mathrm{d}^M\mathcal{J}\int \mathrm{d}^M\boldsymbol{\varphi} \\ \times \mathrm{e}^{-\beta[E_M(\mathcal{J})-\mathrm{i}\Theta_M(\mathcal{J},\boldsymbol{\varphi})]}\mu^*_{M,\mathbf{m}'}(\mathcal{J})\mu_{M,\mathbf{m}}(\mathcal{J}) \\ \times \mathrm{e}^{\mathrm{i}(\mathbf{m}-\mathbf{m}')\cdot\boldsymbol{\varphi}}\big[\mathbf{m}\cdot\boldsymbol{\gamma}_M(\mathcal{J})\big]^2\delta\big[\omega-\mathbf{m}\cdot\boldsymbol{\gamma}_M(\mathcal{J})\big]. \end{aligned} \tag{B26}$$

To partition the spectrum into distinct bands, we must recognise that any term in Eq. (B26) that contributes to the $\Delta n\nu$ band must satisfy $\mathbf{m}\in\mathrm{tot}_M(\Delta n)$, such that $\mathbf{m}\cdot\boldsymbol{\gamma}_M(\mathbf{J}) = \Delta n\Omega + O(\varepsilon)$. Furthermore, conservation of the Matsubara phase ensures that any Fourier component of $\mathrm{e}^{\mathrm{i}\beta\Theta_M(\mathcal{J},\boldsymbol{\varphi})}$ with non-zero frequency must vanish, giving the additional constraint $\mathbf{m}-\mathbf{m}\in\mathrm{tot}_M(0) \implies \mathbf{m}'\in\mathrm{tot}_M(\Delta n)$. It follows that the integrated intensity is given by

$$\begin{aligned} \mathcal{I}^{[M]}_{\Delta n}(\beta) = \frac{\alpha_M\beta|\mathcal{E}|^2}{\hbar Z_M(\beta)}\sum_{\mathbf{m},\mathbf{m}'\in\mathrm{tot}_M(\Delta n)}\int \mathrm{d}^M\mathcal{J}\int \mathrm{d}^M\boldsymbol{\varphi} \\ \times \mathrm{e}^{-\beta[E_M(\mathcal{J})-\mathrm{i}\Theta_M(\mathcal{J},\boldsymbol{\varphi})]}\mu^*_{M,\mathbf{m}'}(\mathcal{J})\mu_{M,\mathbf{m}}(\mathcal{J}) \\ \times \mathrm{e}^{\mathrm{i}(\mathbf{m}-\mathbf{m}')\cdot\boldsymbol{\varphi}}\big[\mathbf{m}\cdot\boldsymbol{\gamma}_M(\mathcal{J})\big]^2, \end{aligned} \tag{B27}$$

In the case of a cubic perturbation, we have $E_M(\mathcal{J}) = E^{(0)}_M(\mathcal{J}) + O(\varepsilon^2)$ as well as $\Theta_M(\mathcal{J},\boldsymbol{\varphi}) = \Theta^{(0)}_M(\mathcal{J},\boldsymbol{\varphi}) + O(\varepsilon^2)$, hence Eq. (B27) can be expanded to second order as

$$\mathcal{I}^{[M]}_{\Delta n}(\beta) = \varepsilon^2 I^{[M]}_{\Delta n}(\beta) + O(\varepsilon^3), \tag{B28}$$

where

$$\begin{aligned} I^{[M]}_{\Delta n}(\beta) = \frac{\alpha_M\beta|\mathcal{E}|^2(\Delta n\Omega)^2}{\hbar Z^{(0)}_M(\beta)}\sum_{\mathbf{m},\mathbf{m}'\in\mathrm{tot}_M(\Delta n)}\int \mathrm{d}^M\mathcal{J}\int \mathrm{d}^M\boldsymbol{\varphi} \\ \times \mathrm{e}^{\mathrm{i}(\mathbf{m}-\mathbf{m}')\cdot\boldsymbol{\varphi}}\mathrm{e}^{-\beta[E^{(0)}_M(\mathcal{J})-\mathrm{i}\Theta^{(0)}_M(\mathcal{J},\boldsymbol{\varphi})]}\lim_{\varepsilon\to0}\frac{1}{\varepsilon^2}\mu^*_{M,\mathbf{m}'}(\mathcal{J})\mu_{M,\mathbf{m}}(\mathcal{J}) \end{aligned} \tag{B29}$$

and

$$Z^{(0)}_M(\beta) = \frac{\alpha_M}{\beta\hbar\Omega}\prod_{k=1}^{\overline{M}}\frac{4\pi^2}{\beta^2\big(\Omega^2+\omega_k^2\big)}. \tag{B30}$$

3. Application to $|\Delta\mathbf{n}| = 2$ bands

For the cubic perturbation of Eq. (3) with $F = 1$, the perturbation to the Matsubara potential is

$$U^{(1)}_M(\mathbf{P},\mathbf{Q}) = \frac{\eta}{6}Q_0^3 + \frac{\eta}{2}Q_0\sum_{k=1}^{\overline{M}}\big(Q_k^2+Q_{-k}^2\big) + \ldots, \tag{B31}$$

which gives

$$\begin{aligned} \widetilde{U}^{(1)}_M\big(\boldsymbol{\mathcal{J}}^{(0)},\boldsymbol{\varphi}^{(0)}\big) &= U^{(1)}_M(\mathbf{P},\mathbf{Q}) \\ &= \sqrt{\frac{2\big(\mathcal{J}^{(0)}_0\big)^3}{9\Omega^3}}\sin^3\big(\varphi^{(0)}_0\big) \\ &+ \sqrt{\frac{2\mathcal{J}^{(0)}_0}{\Omega^3}}\sin\big(\varphi^{(0)}_0\big)\sum_{k=1}^{\overline{M}}\Big[\mathcal{J}^{(0)}_k\sin^2\big(\varphi^{(0)}_k\big)+\mathcal{J}^{(0)}_{-k}\sin^2\big(\varphi^{(0)}_{-k}\big)\Big] \\ &+ \ldots, \end{aligned} \tag{B32}$$

where '…' has been used to denote a sum of centroid-independent terms. Following the standard CPT procedure outlined in Appendix A, we find

$$\begin{aligned} \mathcal{J}^{(0)}_0 = \mathcal{J}_0 - \varepsilon\eta\sqrt{\frac{\mathcal{J}_0}{72\Omega^5}}\sum_{k=-\overline{M}}^{\overline{M}}\mathcal{J}_k \\ \times\Big[6\sin(\varphi_0)-\sin(\varphi_0+2\varphi_k)+3\sin(\varphi_0-2\varphi_k)\Big] \\ + O(\varepsilon^2) \end{aligned} \tag{B33a}$$

$$\begin{aligned} \varphi^{(0)}_0 = \varphi_0 - \frac{\varepsilon\eta}{\sqrt{288\Omega^5\mathcal{J}_0}}\sum_{k=-\overline{M}}^{\overline{M}}\mathcal{J}_k \\ \times\Big[6\cos(\varphi_0)-\cos(\varphi_0+2\varphi_k)+3\cos(\varphi_0-2\varphi_k)\Big] \\ + O(\varepsilon^2), \end{aligned} \tag{B33b}$$

which gives Eq. (48).

The intensity of the first overtone ($\Delta n = 2$) band is obtained by substituting Eq. (48) into Eq. (B29). Using the definitions of $(\boldsymbol{\Pi},\mathbf{X})$ from Eq. (46), this leads to Eq. (52). To make this expression more 'bead-centric', we substitute in the definitions of the bead-like variables $(\boldsymbol{\varpi},\boldsymbol{\chi})$ from Eq. (53), and exploit the cyclic permutational symmetry of the Matsubara distribution (i.e., invariance under the relabelling $l\to l+1$) to yield

$$\begin{aligned} I^{[M]}_{2\nu} = \frac{\pi\eta^2\xi^2|\mathcal{E}|^2\beta}{72M\Omega^6}\sum_{l=1}^{M}\frac{1}{\sqrt{\det(2\pi\boldsymbol{\Sigma})}}\int \mathrm{d}^{2M}\boldsymbol{\Gamma} \\ \times\exp\Big\{-\frac{1}{2}\boldsymbol{\Gamma}\cdot\boldsymbol{\Sigma}^{-1}\boldsymbol{\Gamma}\Big\}(\varpi_0-\mathrm{i}\Omega\chi_0)^2(\varpi_l+\mathrm{i}\Omega\chi_l)^2, \end{aligned} \tag{B34}$$

where

$$\boldsymbol{\Gamma} = \begin{pmatrix}\boldsymbol{\varpi}\\ \boldsymbol{\chi}\end{pmatrix}. \tag{B35}$$

The (complex) covariance matrix is given by

$$\boldsymbol{\Sigma} = \begin{pmatrix}\Omega^2\boldsymbol{\lambda} & \mathrm{i}\boldsymbol{\zeta}\\ \mathrm{i}\boldsymbol{\zeta}^{\mathrm{T}} & \boldsymbol{\lambda}\end{pmatrix}, \tag{B36}$$

where

$$\begin{aligned}\lambda_{l,l'} &= \frac{1}{M\beta}\sum_{k=-\overline{M}}^{\overline{M}}\frac{T_{l,k}T_{l',k}}{\Omega^2+\omega_k^2} \\ &= \frac{1}{\beta}\sum_{k=-\overline{M}}^{\overline{M}}\frac{1}{\Omega^2+\omega_k^2}\cos\left[\frac{2\pi k(l-l')}{M}\right]\end{aligned} \tag{B37a}$$

$$\begin{aligned}\zeta_{l,l'} &= \frac{1}{M\beta}\sum_{k=-\overline{M}}^{\overline{M}}\frac{\omega_k T_{l,-k}T_{l',k}}{\Omega^2+\omega_k^2} \\ &= \frac{1}{\beta}\sum_{k=-\overline{M}}^{\overline{M}}\frac{\omega_k}{\Omega^2+\omega_k^2}\sin\left[\frac{2\pi k(l'-l)}{M}\right].\end{aligned} \tag{B37b}$$

Within each summand of Eq. (B34), for $l' \notin \{0, l\}$ the only dependence on $(\varpi_{l'}, \chi_{l'})$ lies in the Gaussian distribution function of $\mathbf{\Gamma}$. We can therefore immediately integrate these variables out to yield the marginal distribution of $\mathbf{\Gamma}_l = (\varpi_0, \varpi_l, \chi_0, \chi_l)^{\mathrm{T}}$, giving

$$\begin{aligned}I_{2\nu}^{[M]} = \frac{\pi\eta^2\xi^2|\mathcal{E}|^2\beta}{72M\Omega^6}\sum_{l=1}^{M}\frac{1}{\sqrt{\det(2\pi\mathbf{\Sigma}_l)}}\int \mathrm{d}^4\mathbf{\Gamma}_l \\ \times\exp\left\{-\frac{1}{2}\mathbf{\Gamma}_l\cdot\mathbf{\Sigma}_l^{-1}\mathbf{\Gamma}_l\right\}(\varpi_0-\mathrm{i}\Omega\chi_0)^2(\varpi_l+\mathrm{i}\Omega\chi_l)^2,\end{aligned} \tag{B38}$$

where

$$\mathbf{\Sigma}_l = \begin{pmatrix}\Omega^2\lambda_{0,0} & \Omega^2\lambda_{0,l} & 0 & \mathrm{i}\zeta_{0,l} \\ \Omega^2\lambda_{0,l} & \Omega^2\lambda_{l,l} & -\mathrm{i}\zeta_{0,l} & 0 \\ 0 & -\mathrm{i}\zeta_{0,l} & \lambda_{0,0} & \lambda_{0,l} \\ \mathrm{i}\zeta_{0,l} & 0 & \lambda_{0,l} & \lambda_{l,l}\end{pmatrix}. \tag{B39}$$

Integrating out (ϖ_l, χ_l), and simplifying using

$$\Omega^2\lambda_{0,0} = \Omega^2\lambda_{l,l} = \frac{\beta\Omega^2}{M}\sum_{l=1}^{M}\left(\Omega\lambda_{0,l}+\zeta_{0,l}\right)^2 = \frac{1}{\beta^{[M]}}, \tag{B40}$$

leads to Eq. (54) as required.

This result generalises straightforwardly to multidimensional systems, but the algebra is more cumbersome when combination and difference bands are considered. The key result analogous to Eq. (52) that one requires is

$$\begin{aligned}I_{\nu_i\pm\nu_j}^{[M]}(\beta) \propto \left(\Omega_i\pm\Omega_j\right)^2\sum_{k=-\overline{M}}^{\overline{M}}\sum_{k'=-\overline{M}}^{\overline{M}}\int \mathrm{d}^{FM}\mathbf{\Pi}\int \mathrm{d}^{FM}\mathbf{X} \\ \times \mathrm{e}^{-\beta[H_M^{(0)}(\mathbf{\Pi},\mathbf{X})-\mathrm{i}\theta_M(\mathbf{\Pi},\mathbf{X})]} \\ \times\left(\Pi_{i,k}-\mathrm{i}\Omega_i X_{i,k}\right)\left(\Pi_{j,k}\mp\mathrm{i}\Omega_j X_{j,k}\right) \\ \times\left(\Pi_{i,k'}+\mathrm{i}\Omega_i X_{i,k'}\right)\left(\Pi_{j,k'}\pm\mathrm{i}\Omega_j X_{j,k'}\right).\end{aligned} \tag{B41}$$

To obtain the correct prefactor, one also requires

$$\frac{\Omega_i+\Omega_j}{\beta}\sum_{k=-\overline{M}}^{\overline{M}}\frac{\Omega_i\Omega_j+\omega_k^2}{\left(\Omega_i^2+\omega_k^2\right)\left(\Omega_j^2+\omega_k^2\right)} = \frac{\beta_i^{[M]}\Omega_i+\beta_i^{[M]}\Omega_j}{\beta_i^{[M]}\beta_j^{[M]}\Omega_i\Omega_j}, \tag{B42}$$

which is analogous to the last equality of Eq. (B40).

Appendix C: Computational details

1. Gas-phase infrared spectra

a. Quantum calculations

The quantum infrared spectrum of gas-phase water plotted in Fig. 1 was calculated, as in refs. 9 and 25, using Eq. (6) with a set of eigenstates generated by the DVR3D package of Tennyson and co-workers.[55] We employed the PES[63] and DMS[64] due to Partridge and Schwenke. The quantum spectrum of gas-phase ammonia in Fig. 2 was obtained directly using the line list data supplied as supplementary material to ref. 61, calculated using the PES-2 surface and AQZfc DMS described therein. In both cases, the effects of quantum decoherence were mimicked by convolving the spectrum with the function

$$\tilde{f}_{\mathrm{H}}(\omega) = \frac{\pi\sin(w\omega)}{2\omega(\pi^2-w^2\omega^2)}, \tag{C1}$$

where $w = 0.75$ ps. This is equivalent to damping the Kubo-transformed dipole-derivative ACFs using the Hann window[75]

$$f_{\mathrm{H}}(t) = \begin{cases}\cos^2\left(\frac{\pi t}{2w}\right) & |t| \le w \\ 0 & |t| > w.\end{cases} \tag{C2}$$

b. Classical calculations

To obtain the classical spectra of gas-phase water and ammonia, plotted respectively in Figs. 1 and 2, the dipole moments of 100 independent molecules were recorded along 1000 Newtonian trajectories, each of length 1 ps. Prior to each trajectory, the molecules were independently thermalised at 300 K by propagating for an average of 0.1 ps under a local Langevin thermostat[76,77] (OBABO propagator splitting[78]) with friction coefficient 10 ps^{-1}. A time step of 0.125 fs was used throughout. The dipole-derivative ACF was calculated by time averaging over the 10^5 single-molecule Newtonian trajectories. To be consistent with the quantum spectra, each ACF was damped with a Hann window of width $w = 0.75$ ps prior to Fourier transformation.

2. Classical infrared spectrum of liquid water

The classical spectrum of liquid water plotted in Fig. 3 was obtained using the MB-pol PES[49–51] and MB-μ DMS[17] due

to Paesani and co-workers. Eight independent cubic simulation cells of side length 18.6428 Å, each containing 216 water molecules subject to periodic boundary conditions, were first equilibrated at a temperature of 298.15 K by propagating for 250 ps under a global Langevin thermostat[77,79] (BAOAB propagator splitting[78]) with friction coefficient 10 ps^{-1}. The dipole-derivative ACF was calculated for $0 \leq t \leq 0.6$ ps by time averaging over a 100 ps production run in which each cell was propagated under the same conditions as for equilibration. A time step of 0.2 fs was employed throughout, and the ACF was damped with a Hann window of width $w = 0.6$ ps prior to Fourier transformation.

3. Fermi resonance spectra

a. Quantum calculations

To obtain the quantum spectrum included in Figs. 4 and 5, the Hamiltonian $\hat{H}$ of Eq. (64) was diagonalised in the eigenbasis of the harmonic oscillator Hamiltonian $\hat{H}^{(0)}$ of Eq. (65), truncated so as to include only states for which the three vibrational quantum numbers n_1, n_2, n_3 are less than or equal to 10. The Kubo-transformed velocity autocorrelation spectrum of the stretching coordinate, q_1, was then evaluated from the energies and matrix elements of the 50 lowest-energy eigenstates of $\hat{H}$.

b. Matsubara dynamics calculations

The Matsubara forces were computed analytically as described in the supplementary material of ref. 34. To obtain the spectra plotted in the top panel of Fig. 4, the centroid velocity $\dot{Q}_{1,0}$ was recorded along 128000 trajectories of length 10 ps. These were each preceded by propagation for 0.5 ps with a local Langevin thermostat[76,77] attached to each mode (OBABO propagator splitting[78], friction coefficient 0.25 fs^{-1}). A time step of 0.1 fs was used throughout. The Langevin thermostatting enabled sampling of the strictly positive part of the Matsubara distribution, $\mathrm{e}^{-\beta H_M(\mathbf{P},\mathbf{Q})}$, at 150 K. The phase factor, however, had to be accounted for explicitly, using

$$\widetilde{C}^{[M]}_{\dot{q}_1\dot{q}_1}(\beta;t) = \frac{\left\langle \mathrm{e}^{\mathrm{i}\beta\theta_M(\mathbf{P},\mathbf{Q})}\dot{Q}_{1,0}\mathrm{e}^{\mathcal{L}_M t}\dot{Q}_{1,0}\right\rangle_{M,\ \mathrm{p.d.}}}{\left\langle \exp\left\{-\beta\sum_{i,k}\omega_k^2 Q_{i,k}^2/2\right\}\right\rangle_{M,\ \mathrm{p.d.}}} \qquad \text{(C3)}$$

to approximate the Kubo-transformed velocity ACF, where $\langle\ldots\rangle_{M,\ \mathrm{p.d.}}$ denotes an expectation value according to the strictly positive part of the Matsubara distribution. The averaging was performed over time as well as initial conditions. Each ACF was damped with a Gaussian window

$$f_{\mathrm{G}}(t) = \exp\left\{-\frac{t^2}{2w^2}\right\} \qquad \text{(C4)}$$

of width $w = 0.5$ ps, prior to computing the velocity autocorrelation spectrum by Fourier transformation.

c. HD Matsubara calculations

The HD Matsubara spectra were obtained in a similar fashion to the pure Matsubara spectra, from the velocity ACF computed by averaging over 128000 trajectories. However, in this case the initial phase-space points were sampled from the (much simpler) HD Matsubara distribution defined in Section IV A; the phase is accounted for implicitly (albeit approximately) within this distribution, so did not need to be averaged over explicitly as in the pure Matsubara simulations (see Eq. (C3)). Furthermore, since Matsubara trajectories do not rigorously conserve the HD distribution, time averaging could not be performed, hence the ACFs were computed by averaging over the initial conditions only.

d. Classical dynamics with imitated Matsubara heating

The classical dynamics with Matsubara heating was algorithmically equivalent to HD Matsubara with M set to unity, except that the sampling of each pair of dynamical variables was performed at the appropriate Matsubara effective temperature $T_i^{[M]} = 1/k_{\mathrm{B}}\beta_i^{[M]}$ (rather than the actual temperature $T = 1/k_{\mathrm{B}}\beta$). Furthermore, because (p_i, q_i) represent, in this case, approximations to the dynamical variables of a Matsubara 'bead', the resulting spectra had to be scaled by $\beta_1^{[M]}/\beta$ relative to those obtained from centroid trajectories (such that the spectral intensities are comparable to those of HD Matsubara calculations).

[1] I. R. Craig and D. E. Manolopoulos, J. Chem. Phys. **121**, 3368 (2004).
[2] T. E. Markland and D. E. Manolopoulos, J. Chem. Phys. **129**, 024105 (2008).
[3] S. Habershon, D. E. Manolopoulos, T. E. Markland, and T. F. Miller III, Ann. Rev. Phys. Chem. **64**, 387 (2013).
[4] J. Cao and G. A. Voth, J. Chem. Phys. **100**, 5106 (1994).
[5] G. A. Voth, Adv. Chem. Phys. **93**, 135 (1996).
[6] M. Rossi, M. Ceriotti, and D. E. Manolopoulos, J. Chem. Phys. **140**, 234116 (2014).
[7] K. K. G. Smith, J. A. Poulsen, G. Nyman, A. Cunsolo, and P. J. Rossky, J. Chem. Phys. **142**, 244113 (2015).
[8] T. J. H. Hele, Mol. Phys. **115**, 1435 (2017).
[9] G. Trenins, M. J. Willatt, and S. C. Althorpe, J. Chem. Phys. **151**, 054109 (2019).
[10] N. Boekelheide, R. Salomón-Ferrer, and T. F. Miller, Proc. Natl. Acad. Sci. U. S. A. **108**, 16159 (2011).
[11] J. S. Kretchmer and T. F. Miller, J. Chem. Phys. **138** (2013).
[12] S. Habershon, G. S. Fanourgakis, and D. E. Manolopoulos, J. Chem. Phys. **129**, 074501 (2008).
[13] S. Habershon, T. E. Markland, and D. E. Manolopoulos, J. Chem. Phys. **131**, 024501 (2009).
[14] S. Habershon and D. E. Manolopoulos, J. Chem. Phys. **131**, 244518 (2009).
[15] F. Paesani and G. A. Voth, J. Phys. Chem. B **113**, 5702 (2009).
[16] M. Rossi, H. Liu, F. Paesani, J. M. Bowman, and M. Ceriotti, J. Chem. Phys. **141**, 181101 (2014).
[17] G. R. Medders and F. Paesani, J. Chem. Theory Comput. **11**, 1145 (2015).
[18] S. K. Reddy, D. R. Moberg, S. C. Straight, and F. Paesani, J. Chem. Phys. **147**, 244504 (2017).
[19] O. Marsalek and T. E. Markland, J. Phys. Chem. Lett. **8**, 1545 (2017).
[20] K. M. Hunter, F. A. Shakib, and F. Paesani, J. Phys. Chem. B **122**, 10754 (2018).
[21] M. J. Willatt, M. Ceriotti, and S. C. Althorpe, J. Chem. Phys. **148**, 102336 (2018).
[22] K. A. Jung, P. E. Videla, and V. S. Batista, J. Chem. Phys. **148**, 244105 (2018).

[23] Q. Yu and J. M. Bowman, J. Phys. Chem. A **123**, 1399 (2019).
[24] Y. Litman, J. Behler, and M. Rossi, Faraday Discuss. **221**, 526 (2019).
[25] R. L. Benson, G. Trenins, and S. C. Althorpe, Faraday Discuss. **221**, 350 (2019).
[26] Z. Tong, P. E. Videla, K. A. Jung, V. S. Batista, and X. Sun, J. Chem. Phys. **153** (2020).
[27] V. Kapil, D. M. Wilkins, J. Lan, and M. Ceriotti, J. Chem. Phys. **152** (2020).
[28] G. Trenins and S. C. Althorpe, J. Chem. Phys. **149**, 014102 (2018).
[29] A. Witt, S. D. Ivanov, M. Shiga, H. Forbert, and D. Marx, J. Chem. Phys. **130**, 194510 (2009).
[30] S. D. Ivanov, A. Witt, M. Shiga, and D. Marx, J. Chem. Phys. **132**, 031101 (2010).
[31] These shifts can be much larger in strongly anharmonic potentials; see ref. 23.
[32] T. Plé, S. Huppert, F. Finocchi, P. Depondt, and S. Bonella, J. Chem. Phys. **submitted** (2021).
[33] T. Plé, *Nuclear Quantum Dynamics: exploration and comparison of trajectory-based methods*, Ph.D. thesis, Sorbonne Université (2020).
[34] T. J. H. Hele, M. J. Willatt, A. Muolo, and S. C. Althorpe, J. Chem. Phys. **142**, 134103 (2015).
[35] K. A. Jung, P. E. Videla, and V. S. Batista, J. Chem. Phys. **151**, 034108 (2019).
[36] T. J. H. Hele, M. J. Willatt, A. Muolo, and S. C. Althorpe, J. Chem. Phys. **142**, 191101 (2015).
[37] T. J. H. Hele, Mol. Phys. **114**, 1461 (2016).
[38] G. Trenins, *Quasicentroid Molecular Dynamics*, Ph.D. thesis, University of Cambridge (2020).
[39] K. A. Jung, P. E. Videla, and V. S. Batista, J. Chem. Phys. **153**, 124112 (2020).
[40] H. Wang, X. Sun, and W. H. Miller, J. Chem. Phys. **108**, 9726 (1998).
[41] X. Sun, H. Wang, and W. H. Miller, J. Chem. Phys. **109**, 7064 (1998).
[42] X. Sun, H. Wang, and W. H. Miller, J. Chem. Phys. **109**, 4190 (1998).
[43] W. H. Miller, J. Phys. Chem. A **105**, 2942 (2001).
[44] Q. Shi and E. Geva, J. Phys. Chem. A **107**, 9059 (2003).
[45] J. A. Poulsen, G. Nyman, and P. J. Rossky, J. Chem. Phys. **119**, 12179 (2003).
[46] J. Liu and W. H. Miller, J. Chem. Phys. **131**, 074113 (2009).
[47] J. Liu, W. H. Miller, G. S. Fanourgakis, S. X. Xantheas, S. Imoto, and S. Saito, J. Chem. Phys. **135**, 244503 (2011).
[48] J. Liu, Int. J. Quantum Chem. **115**, 657 (2015).
[49] V. Babin, C. Leforestier, and F. Paesani, J. Chem. Theory Comput. **9**, 5395 (2013).
[50] V. Babin, G. R. Medders, and F. Paesani, J. Chem. Theory Comput. **10**, 1599 (2014).
[51] G. R. Medders, V. Babin, and F. Paesani, J. Chem. Theory Comput. **10**, 2906 (2014).
[52] QCMD calculations of gas-phase ammonia and MB-pol/MB-μ liquid water have not yet been reported in the literature.
[53] H. Goldstein, C. Poole, and J. Safko, *Classical Mechanics*, 3rd ed. (Addison–Wesley, New York, 2002).
[54] M. Basire, F. Mouhat, G. Fraux, A. Bordage, J. L. Hazemann, M. Louvel, R. Spezia, S. Bonella, and R. Vuilleumier, J. Chem. Phys. **146**, 134102 (2017).
[55] J. Tennyson, M. A. Kostin, P. Barletta, G. J. Harris, O. L. Polyansky, J. Ramanlal, and N. F. Zobov, Comput. Phys. Commun. **163**, 85 (2004).
[56] J. J. Sakurai and J. Napolitano, *Modern Quantum Mechanics*, 2nd ed. (Cambridge University Press, Cambridge, 2017).
[57] M. E. Tuckerman, *Statistical Mechanics: Theory and Molecular Simulation* (Oxford University Press, Oxford, 2010).
[58] Since we are not interested in vibration-rotation coupling, we treat the dipole moment as a scalar quantity to avoid cumbersome algebra; more formally, μ represents just one component of the dipole moment vector in the body-fixed frame of the molecule.
[59] Following the usual assumption that the frequency dependence of the refractive index is negligible.
[60] S. J. Yao and J. Overend, Spectrochim. Acta Part A Mol. Spectrosc. **32**, 1059 (1976).
[61] S. N. Yurchenko, R. J. Barber, A. Yachmenev, W. Thiel, P. Jensen, and J. Tennyson, J. Phys. Chem. A **113**, 11845 (2009).
[62] Although the results of ref. 32 and Section II were derived assuming a linear DMS, it was shown in ref. 60 that the quantum integrated intensities have the same temperature dependence (to leading order) when one accounts for quadratic terms. Thus the correction factor of Eq. (13) is applicable even when the DMS is weakly non-linear.
[63] H. Partridge and D. W. Schwenke, J. Chem. Phys. **106**, 4618 (1997).
[64] D. W. Schwenke and H. Partridge, J. Chem. Phys. **113**, 6592 (2000).
[65] J. E. Bertie and Z. Lan, Appl. Spectrosc. **50**, 1047 (1996).
[66] D. M. Ceperley, Rev. Mod. Phys. **67**, 279 (1995).
[67] Note that this spectrum must be regarded as an approximation to the Raman spectrum, as the symmetric stretch vibration of CO_2 is not infrared active.
[68] A canonical PT analysis along the lines of Section III is presumably possible, but would be long and involved as one is required to deal with quasi-degeneracy in the reference system.
[69] S. Karsten, S. D. Ivanov, S. I. Bokarev, and O. Kühn, J. Chem. Phys. **149**, 194103 (2018).
[70] This is easily proved by noting that functions that are odd powers of $P_{i,k}$ or $Q_{i,k}$, with $k > 0$, are antisymmetric with respect to imaginary-time inversion.
[71] One must take care to avoid propagating long trajectories, since the Matsubara dynamics conserves the exact distribution, not the decorrelated distribution.
[72] X. Liu and J. Liu, Mol. Phys. **116**, 755 (2018).
[73] The success of first-order PT in recovering the overtone and combination intensities suggests that it might be possible to obtain accurate predictions of infrared spectra simply by carrying out classical MD and using higher order PT to generate corrections to the frequencies.
[74] *Mathematica, Version 12.0* (Wolfram Research, Inc., Champaign, IL, 2019).
[75] W. H. Press, S. A. Teukolsky, W. T. Vetterling, and B. P. Flannery, *Numerical Recipes in Fortran 77: The Art of Scientific Computing*, 2nd ed. (Cambridge University Press, 1992).
[76] G. Bussi and M. Parrinello, Phys. Rev. E **75**, 056707 (2007).
[77] G. Bussi and M. Parrinello, Comput. Phys. Commun. **179**, 26 (2008).
[78] B. Leimkuhler and C. Matthews, Appl. Math. Res. eXpress **2013**, 34 (2013).
[79] G. Bussi, D. Donadio, and M. Parrinello, J. Chem. Phys. **126**, 014101 (2007).